

BRAIN-be 2.0

**Belgian Research Action
through Interdisciplinary
Networks**

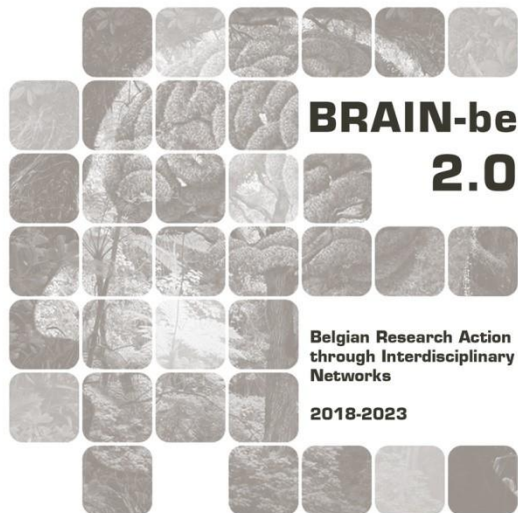
2018-2023

SWiM

Solar wind modelling with EUHFORIA for new heliophysics space missions

Jasmina Magdalenic, Senthamizh Pavai Valliappan, Immanuel Christopher Jebaraj, Evangelia Samara, Luciano Rodriguez, Ketaki Deshpande Brenda Walsh, (Observatoire Royal du Belgique)

Stefaan Poedts, Jasmina Magdalenic, Angelo Valentino, Anwasha Maharana, (CmPA - KU Leuven, Belgium)



NETWORK PROJECT

SWiM

Solar wind modelling with EUFORIA for new heliophysics space missions

Contract - B2/191/P1/SWiM

FINAL REPORT

(project duration 2019 -2024)

PROMOTORS: Jasmina Magdalenic (Observatoire Royal du Belgique & KULeuven, Belgium)
Stefaan Poedts (KULeuven, Belgium)

AUTHORS:

Jasmina Magdalenic - PI (Observatoire Royal du Belgique & CmPA – KULeuven, Belgium)
Senthamizh Pavai Valliappan, Ketaki Deshpande, Brenda Dorsch, Luciano Rodriguez
(Observatoire Royal du Belgique)
Immanuel Jebaraj, Evangelia Samara (at the time of the project at Observatoire Royal du
Belgique)

Stefaan Poedts - PI (CmPA – KULeuven, Belgium)
Anwsha Maharana (at the time of the project at CmPA – KULeuven, Belgium)
Angelo Valentino, Baratashvili, Tinatin, Michaela Brchnelova, Christin Verbeke, Antonio
Niemela (CmPA – KULeuven, Belgium)



Published in 2025 by the Belgian Science Policy Office
WTCIII
Simon Bolivarlaan 30 bus 7
Boulevard Simon Bolivar 30 bte 7
B-1000 Brussels
Belgium
Tel: +32 (0)2 238 34 11
<http://www.belspo.be>
<http://www.belspo.be/brain-be>

Contact person: Jasmina Magdalenic
Tel: +32 (0)2 7903964

Neither the Belgian Science Policy Office nor any person acting on behalf of the Belgian Science Policy Office is responsible for the use which might be made of the following information. The authors are responsible for the content.

No part of this publication may be reproduced, stored in a retrieval system, or transmitted in any form or by any means, electronic, mechanical, photocopying, recording, or otherwise, without indicating the reference:

Jasmina Magdalenic, Senthamizh Pavai Valliappan, Ketaki Deshpande, Brenda Dorsch, Luciano Rodriguez, Immanuel Jebaraj, Evangelia Samara. ***Solar wind modeling with EUHFORIA for new heliophysics space missions***. Final Report. Brussels: Belgian Science Policy Office 2025 – 37 p. (BRAIN-be 2.0 - (Belgian Research Action through Interdisciplinary Networks))

TABLE OF CONTENTS

ABSTRACT	5
1. INTRODUCTION	5
2. STATE OF THE ART AND OBJECTIVES	6
3. METHODOLOGY	7
4. SCIENTIFIC RESULTS AND RECOMMENDATIONS	8
5. DISSEMINATION AND VALORISATION	33
6. PUBLICATIONS	34
7. ACKNOWLEDGEMENTS	37
ANNEXES	37

ABSTRACT

The solar atmosphere is a dynamic and complex plasma system that generates solar wind, a continuous outflow of plasma filling the heliosphere. Solar wind and its transient structures, such as coronal mass ejections (CMEs), may generate space weather disturbances that can affect human life and modern technological society. This makes the studies of solar wind and CMEs a key topic in solar physics and space weather research.

The constantly changing properties of the solar wind plasma and its transients were up to now poorly constrained by observations, as the in-situ measurements were routinely taken only at 1 au. The novel and recently available observations by Parker Solar Probe (PSP) and Solar Orbiter (SoLO) sample the solar wind properties at different locations between the Sun and 1 au and allow validation of the models of solar wind and CMEs. The main importance in the modelling of solar wind dynamics lies in the 3D presentation of the solar wind and its transients that can be provided by the models, allowing in such a way also prediction of the arrival of these transients at Earth or other points in the inner heliosphere.

The SWiM project is focused on studying the novel in situ observations at different points of the inner heliosphere and employ them in the validation of the EUHFORIA model (European Heliospheric Forecasting Information Asset, see Pomoell & Poedts 2018). Together with the validation of this 3D MHD model of solar wind and CMEs in the framework of SWiM project we also developed alternative models such a ICARUS, COCONUT and CME model horse-show.

Keywords: solar wind, coronal mass ejections (CMEs) in situ data, PSP data, Solar Orbiter data, EUHFORIA, COCONUT, Icarus.

1. INTRODUCTION

The Sun is our closest star, and this proximity enables us to observe readily its surface activity and the effects of this activity in the interplanetary space (heliosphere). The solar atmosphere is a dynamic and complex plasma system that generates solar wind, a continuous outflow of plasma filling the heliosphere. The outermost layer of the solar atmosphere, the corona, is the region in which the most energetic transient processes in the solar system, flares and coronal mass ejections (CMEs) occur. CMEs are large amounts of plasma and magnetic flux expelled from the Sun into the interplanetary medium. Fast solar wind and especially CMEs may generate space weather disturbances that can affect human life and especially modern technological society (satellite operations, navigation systems, radio communications, etc., see Bothmer & Daglis 2006).

Therefore, studies of the solar wind and of CMEs are a key topic in solar physics and space weather research. Properties of the solar wind plasma (density, temperature, magnetic field) change on the way from the Sun to the Earth, and this process is now poorly constrained by observations. Direct (in situ) measurements by spacecraft provide one or several one-dimensional cuts through the solar wind structure and through the CME volume. This is insufficient to derive the three-dimensional extent of the fast solar wind and full three-dimensional structure of CMEs (e.g. Jacobs et al. 2009; Hinterreiter et al., 2019). Moreover, in-situ measurements were so far routinely taken only at 1 AU (astronomical unit), which is not sufficient to constrain the evolution of the solar wind and its structures on the way from the Sun to the Earth. Therefore, we need to rely on models, which are still not realistic enough to predict, with sufficient accuracy, the arrival of high-speed streams (HSS) at the Earth or magnetic configuration of CMEs. Present state-of-the-art models of the background solar wind and CME propagation in the heliosphere, in particular EUHFORIA (European Heliospheric Forecasting Information Asset, see Pomoell & Poedts 2018), are driven using solar remote-sensing observations as input. Recent testing of the solar wind modelling with EUHFORIA (Hinterreiter et al. 2019; Asvestari et al. 2019) paved the way to the optimization of the model abilities to predict solar wind, but only at 1 AU. The SWiM project was focused on studying novel in situ observations at different points of the inner heliosphere, primarily by the NASA's Parker Solar Probe (PSP, Fox et al. 2016) and ESA's Solar Orbiter (SoO, Müller et al. 2013), and employ them to validate EUHFORIA model. Additionally, to the validation of EUHFORIA model in the framework of the SWiM project we also developed alternative models of solar wind and CMEs

2. STATE OF THE ART AND OBJECTIVES

During last several decades a lot of efforts was invested in creation and improvements of the solar wind and the CME models with the aim of accurate forecast of their arrival to Earth. The two, most frequently used state-of-the-art magnetohydrodynamical models (MHD models) of the background solar wind and CME propagation in the heliosphere are EUHFORIA and ENLIL (Odstrcil et al, 1996, 2005). Due to EUHFORIA's flexibility (separate coronal and heliospheric part) different parts of the model are being continuously improved (e.g. Hinterreiter et al, 2019; Asvestari et al, 2019; Samara et al, 2021; Maharana et al, 2022). Presently, despite the fast development of the solar wind and CME models the estimation of the solar wind plasma characteristics and arrival of the high-speed streams and CMEs at Earth is still not realistic enough. The novel PSP and Solar Orbiter observations provide unique tools for the validation of the models at different distances from the Sun, which was up to now not possible up to this large extent. The SWiM project is focused on studying this novel in situ observations at different points of the inner heliosphere and employ them to validate EUHFORIA model.

To achieve its objectives, the SWiM project brings together two world-class leaders in solar physics: CmPA/KUL (expert in modelling) and SIDC/ROB (expert in observations and space weather forecasting). Present state-of-the-art models of the background solar wind and CME propagation in the heliosphere, and in particular EUHFORIA, are driven using solar remote-sensing observations as input. The EUHFORIA modelling was, in the framework of the SWiM project, constrained at a large number of locations widely spaced in radial distance and heliospheric longitude through novel PSP and Solar Orbiter observations.

The project was very timely as it brought together the best heliospheric simulations and the most novel observations. The improved EUHFORIA is being used in the operational space weather forecasting at the Regional Warning Center Belgium hosted by ROB.

The overarching science question addressed in the SWiM project is: *how does solar wind evolve and define its space weather impact on Earth?*

To address this question, the main specific objectives of the project are:

- 1) to simulate the background solar wind and CME propagation using a state-of-the-art model,
- 2) to compare the simulation results to novel in situ observations of the solar wind by PSP and Solar Orbiter,
- 3) to improve and optimize the EUHFORIA model for scientific and forecasting purposes.

3. METHODOLOGY

The primary focus of the SWiM project were validation and improvements of the EUHFORIA model and data constrained modelling at the close to the Sun distances, therefore we first present the main information about the model. Additionally, to the EUHFORIA model that was foreseen to be employed for the solar wind modelling, partially in the framework of this project we also developed two new solar wind models COCONUT and ICARUS (see Section 4).

3.1 EUHFORIA (European Heliospheric Forecasting Information Asset) model

Majority of presently used solar wind and CME models lack some key characteristics in order to provide accurate forecasts of the coronal and heliospheric conditions. In particular, none of the presently available models (e.g. WSA-ENLIL etc.) is able to predict the magnetic structure of CMEs, and accordingly the strength of the geomagnetic impact, the stand-off distance of the associated shock wave, or the properties of solar energetic particle (SEP) events. In order to address this growing need for accurate space weather predictions, a new model named EUHFORIA was developed by KU Leuven and University of Helsinki.

EUHFORIA is a very flexible model consisting of three essential parts: a) coronal model, b) heliospheric model and c) eruption model responsible for insertion of CMEs. The main purpose of the *coronal model* is to provide the inner boundary conditions necessary for the initiation of the heliospheric part. In the default EUHFORIA set-up (the same as in Pomoell & Poedts, 2018), the MHD wind parameters at 0.1 au are provided with the semi-empirical Wang-Sheeley-Arge (WSA; Arge et al. 2003, 2004) model, in combination with the potential field source surface (PFSS) model (Altschuler & Newkirk 1969; Wiegmann et al. 2017) and the Schatten current sheet (SCS) model (Schatten et al. 1969). Using these initial boundary conditions in an MHD relaxation procedure, we obtain a steady heliospheric background wind.

The task of the *heliospheric model* is to compute the time-dependent evolution of the plasma from the inner boundary of EUHFORIA to the distance of typically up to 2 au. This is done by numerically solving the MHD equations with the boundary conditions provided by the coronal model. In the default set up of EUHFORIA the CMEs are injected at the interface radius determined by the eruption model. Thus, from 0.1 au onwards, EUHFORIA provides a time-dependent, three-dimensional model of the heliosphere that self-consistently captures effects such as solar wind stream interactions, shock formation and the interaction of CMEs with structures in the solar wind. An important feature of EUHFORIA is its flexibility, namely the three models are fully autonomous and each part of EUHFORIA can be easily substituted with other model in a modular way, e.g. it is possible to replace the coronal model or the eruption model. This characteristic of EUHFORIA is particularly important and it was strongly employed in this project.

After the magnetogram insertion EUHFORIA employs the PFSS model until the height of $2.6 R_{\odot}$, to reconstruct a current-free magnetic field (Fig. 1a). Starting from the height of $2.3 R_{\odot}$ onwards, the SCS model is used. This model starts before the end of the PFSS domain in order to reduce possible kinks in the magnetic field lines due to incompatible boundary conditions between the two models (see e.g. McGregor et al. 2011; Asvestari et al. 2019). The purpose of the SCS is to create an approximately uniform coronal magnetic field away from the Sun, maintaining a thin structure for the heliospheric current sheet (HCS). A more uniform magnetic field is necessary in order to obtain a better agreement between the model and the

observations. The initial version of the CME model in EUHFORIA consists of a hydrodynamic cone-like model whose parameters (width, speed, direction) were constrained from fitting the cone to coronal imaging observations of CMEs. Recently, few more advanced CME models were implemented in EUHFORIA. The improvements and modifications of EUHFORIA, as well as the validation of the model are planned to be performed within the SWiM project.

4. SCIENTIFIC RESULTS AND RECOMMENDATIONS

The work performed in the framework of the SWiM project was presented in many publications in the refereed journals and here we give the brief overview of some of them, sorted out in the several groups of topics. The list of the publications can be found at the end of this report.

4.1 Modeling of the background solar wind with EUHFORIA

Even if modelling of the background solar wind was addressed in a majority of the here listed publications, we first present the one that have the main focus in the solar wind modelling.

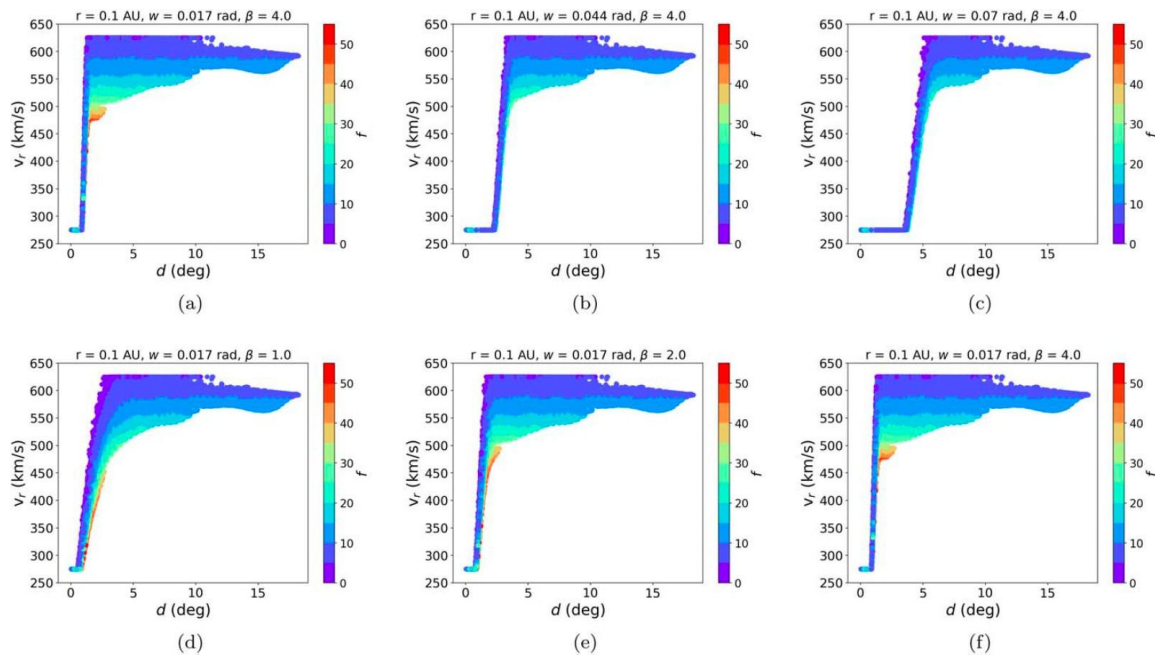


Figure 1. Behaviour of some of the parameters in the WSA formula. Radial velocity at the boundary as a function of the distance to the coronal hole boundary. From panels (a) to (c), parameter w increases while parameter β stays fixed. From panels (d) to (e), β increases as w stays fixed. The flux-tube expansion factor is colour coded.

4.1.1 Influence of coronal hole morphology on the solar wind speed at Earth

This work was presented in the publication: Samara, E., Magdalenic, J., Rodriguez, L. et al., 2022, *Astronomy & Astrophysics*.

It has long been known that the high-speed stream (HSS) peak velocity at Earth directly depends on the area of the coronal hole (CH) on the Sun. Different degrees of association between the two parameters have been shown by many authors. This extended study revisited the association in greater detail for a sample of 45 nonpolar CHs during the minimum phase of solar cycle 24, with the aim to understand how CHs of different properties

influence the HSS peak speeds observed at Earth and draw from this to improve solar wind modeling with EUHFORIA.

Our results show that the morphological parameters of CHs such as the aspect ratio, orientation angle, and complexity play a major role in determining the HSS peak speed at 1 AU, and they need to be taken into consideration for empirical models, such as WSA model used in the default set up of EUHFORIA, that aim to forecast the fast solar wind at Earth based on the observed CH solar sources.

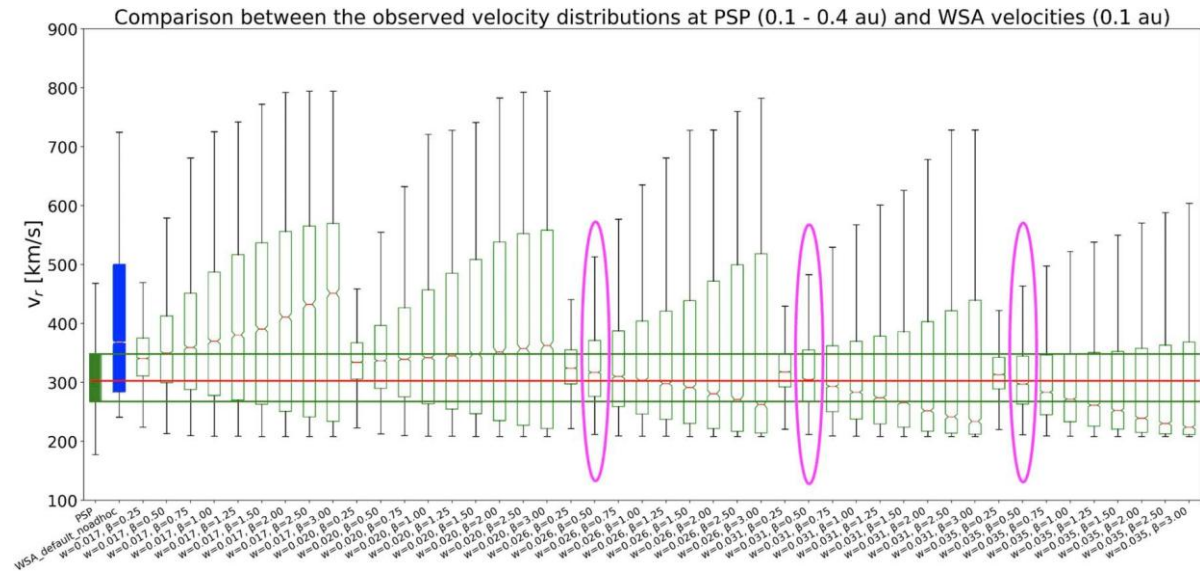


Figure 2. Box-whisker plot of velocities distributions. Green box: velocity values recorded by PSP between 0.1 and 0.4 au for all the first eight encounters. Blue box: WSA velocities at 0.1 au without the ad hoc modifications. All other boxes reflect the WSA velocity distributions resulted out of the parametric study of $[w, \beta]$. The median value of each distribution is shown in red, while the first and third quartiles are represented by the lower and upper box edges, respectively. The black legs extending above and below the boxes show the maximum and minimum velocity values of those distributions. Distributions circled in magenta resemble the PSP (green) distribution the best.

4.1.2 Calibrating the WSA Model in EUHFORIA Based on Parker Solar Probe Observations

This work was presented in the publication: Samara, E., Arge, C. N., Pinto, R. F. et al., 2024, The Astrophysical Journal, and it is the study that straight forward connects to the study presented in Section 4.1.1.

In order to improve solar wind modeling with EUHFORIA code we employed PSP observations during the latest solar minimum period (years 2018–2021) to calibrate the version of the WSA formula used in the coronal model of the default set up of EUHFORIA (see Fig.1). WSA provides a set of boundary conditions at 0.1 au necessary to initiate the heliospheric part of EUHFORIA, namely, the domain extending beyond the solar Alfvénic point. To calibrate WSA, we observationally constrain four constants in the WSA semiempirical formula based on PSP observations. We show how the updated (after the calibration) WSA boundary conditions at 0.1 au are compared to PSP observations at similar distances, and we further propagate these conditions in the heliosphere according to EUHFORIA's MHD approach (see Fig.2). We assess the predictions at Earth based on the dynamic time-warping technique. Our findings suggest that, for the period of interest, the WSA configurations that

resembled optimally the PSP observations close to the Sun were different from the ones needed to provide better predictions at Earth. One reason for this discrepancy can be attributed to the scarcity of fast solar wind velocities recorded by PSP. The calibration of the model was performed based on unexpectedly slow velocities that did not allow us to achieve generally and globally improved solar wind predictions compared to older studies. Other reasons can be attributed to missing physical processes from the heliospheric part of EUHFORIA but also the fact that the currently employed WSA relationship, as coupled to the heliospheric MHD domain, may need a global reformulation beyond that of just updating the four constant factors that were taken into account in this study.

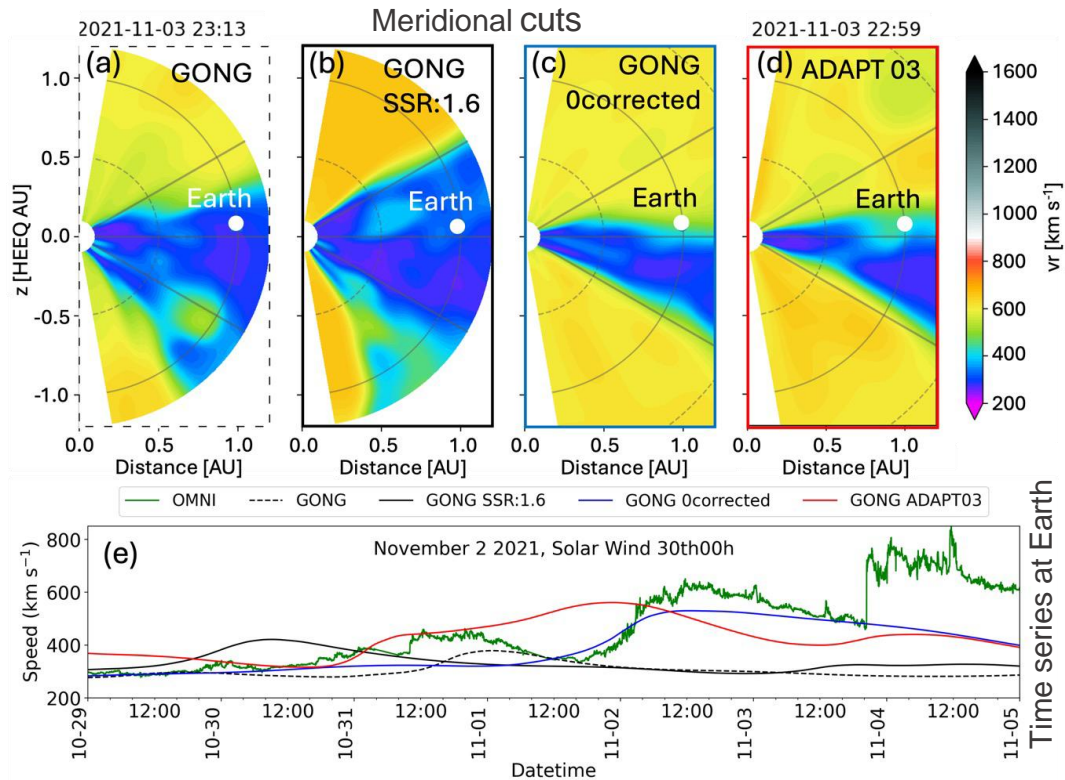


Figure 3. The solar wind modelling results of EUHFORIA for the three different set up, in the 2D meridional cuts at Earth (top panel), and the 1D time series compared with the in situ solar wind speed (bottom panel). We see that, even if the time series show improvements in the modelling results when ADAPT map (realization 03) was used as an input to EUHFORIA, the solar wind originating from the polar coronal holes is strongly overestimated, as visible in the 2D domain.

4.1.3 Optimization of the Solar Wind modelling with EUHFORIA

Results of this work were presented at different conferences and will be also presented in the manuscript that is to be submitted to Astronomy & Astrophysics, Valentino, A., Magdalenic, J., Deshpande, K.

In this study we address the importance of the optimization of the solar wind modelling with EUHFORIA for the accurate modelling of CMEs. We analyse two solar eruptive events: on December 07, 2020 and on November 02, 2021. Both events were associated with full halo coronal mass ejections (CMEs) and flares. The in situ times series at Earth, show that the arrival of the CME was following slow solar wind, for the 1st event, while the 2nd arrived after the fast solar wind. In both cases, the accurate solar wind modelling was crucial for accurate

modelling of CMEs. We employ different magnetogram inputs: GONG synoptic maps and ADAPT maps and vary the parameters in the PFSS part of the coronal model of EUHFORIA to and show how large is the difference in the CME arrival times using these different model set-ups. We also show the large importance of the polar coronal holes not only for the accurate solar wind modelling but also for the accurate modelling of the CME arrival time. The example of three different set up and the accuracy of the solar wind modelling in the 2D meridional cuts at Earth, and the 1D time series compared with the in situ solar wind speed are presented in the Fig.3.

4.1.4 Solar Wind modelling with EUHFORIA at the PSP distances

Results of this work were presented at different conferences and will be also presented in the manuscript that is in the submission process in Astronomy & Astrophysics: Solar wind modeling with EUHFORIA and comparison with the PSP observations, by Senthamizh, P. V., J. Magdalenic, J., Rodriguez, L., Poedts, S., and Samara, E.

In this extended study we present the modelling results with EUHFORIA at the close to the Sun - PSP distances, for the first 10 PSP close encounters. We show that the modelling results for obtained averaging the daily run can significantly deviate when even the subsequent daily solar wind runs are considered (Fig. 4). We also found out that it is very important to look at the modelling results not only at the specific point in the space (where we have in situ observations) but also to consider the time series at close-by positions. This result was further inspected in the study presented in the Section 4.1.3.

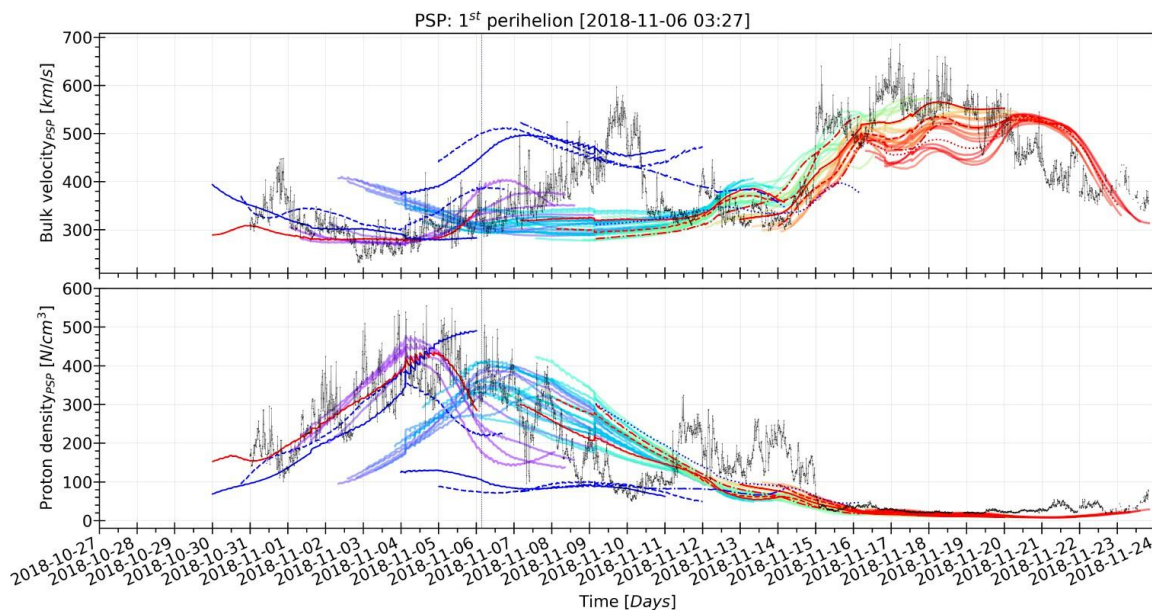


Figure 4. Comparison of the solar wind speed (top panel) and density (bottom panel) observed by PSP during its first perihelion passage and daily EUHFORIA simulation results (colourful curves). We note significant spread of modelling results for some of the subsequent daily runs.

The Figs. 5 and 6 show some of the statistics of the modelling results of EUHFORIA at close to the Sun distances compared with the PSP in situ data. The dominance of the green coloured regions (Fig 6) which represent the solar wind velocity larger than the ambient PSP velocity increased for the 20% of its value, indicates that the solar wind velocity modelled by EUHFORIA is generally overestimated at the close to the Sun distances. This result is

opposite to the one obtained by Hinterreiter et al., (2019), for the close to Earth distances where the authors found strong underestimation of the modelled solar wind velocity and overestimation of the modelled solar wind plasma density. Once again, we have noticed that the coronal model of EUHFORIA, as well as the magnetogram input to EUHFORIA are among the main characteristics influencing accuracy of the solar wind modelling.

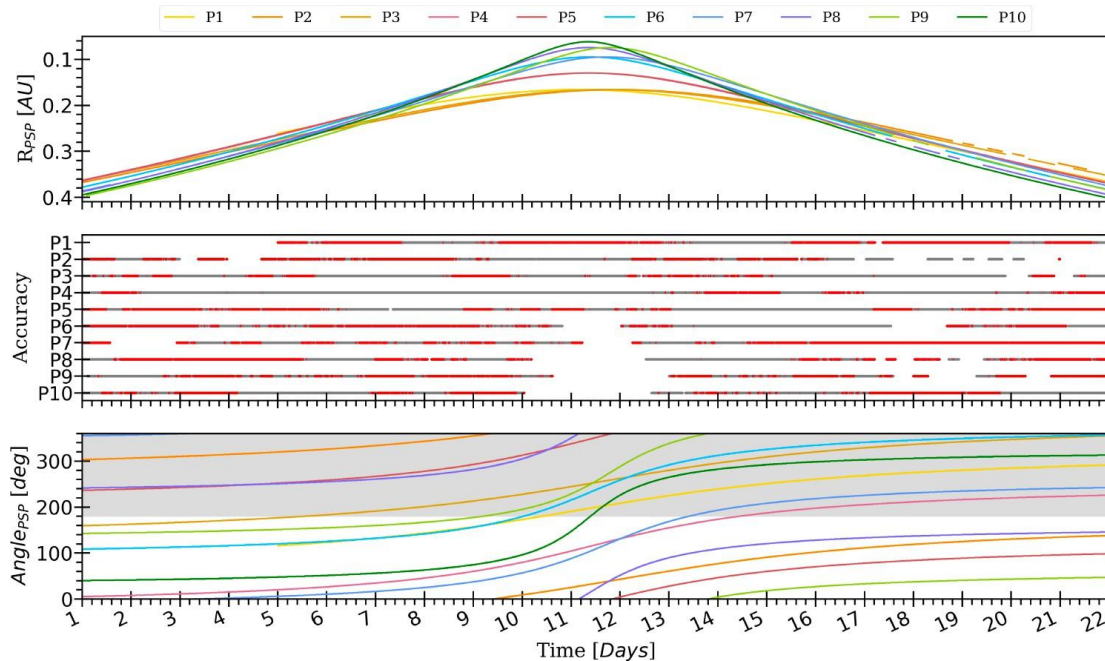


Figure 5. The radial distance of the PSP from the Sun during its first ten perihelion encounters (top panel). The calculated accuracy of EUHFORIA simulation for the first ten perihelion encounters (middle panel). The EUHFORIA simulation accuracy is good (red circles) if the combined EUFORIA data falls within the 20% margin of solar wind speed data, otherwise it is bad (gray circles). The angle of PSP with respect to the East limb of the Sun (bottom panel). The angles 0 – 180 corresponds to the location of the PSP at the front side of the Sun, while angles greater than that corresponds to the far side which is shaded grey.

4.1.5 Quantifying the Expanding and Cooling Effects into the Double Adiabatic Evolution of the Solar Wind Through the Expanding Box Model

This work was presented in the publication: Echeverría-Veas, S., Moya, P. S., Lazar, M. et al., 2024, The Astrophysical Journal.

One of the fundamental problems in space physics is the expansion dynamics of the solar wind, strongly correlated with collective plasma reactions, such as wave instabilities that tend to relax kinetic anisotropies. The expansion is in general described through the double adiabatic or Chew–Goldberger–Low (CGL) theory, which sets the main ideas and plasma expansion's major role in describing plasma cooling/heating dynamics. Here, using the expanding box model (EBM) we revisit the CGL description including plasma expansion. Our primary objective is to isolate the expanding effects into the conservation of the double adiabatic invariants, a key aspect of the CGL theory. Following the same approximations and assumptions as in EBM and CGL theory, we developed a CGL-like description in which expansion modifies conservation of the double adiabatic invariants. Our results show that the double adiabatic equations are no longer conserved if plasma cooling is introduced through the EBM, with explicit dependence on expanding parameters, magnetic field profiles, and velocity gradients. Solving the equations for different magnetic field and density profiles

(obtained self-consistently through the equations), we compute the evolution of temperature anisotropy and plasma beta, which deviates from CGL predictions and empirical observations. This deviation is attributed to the plasma cooling effect induced by the expansion of the plasma. The results suggest that heating mechanisms even play a major role in counteracting plasma cooling during expansion.

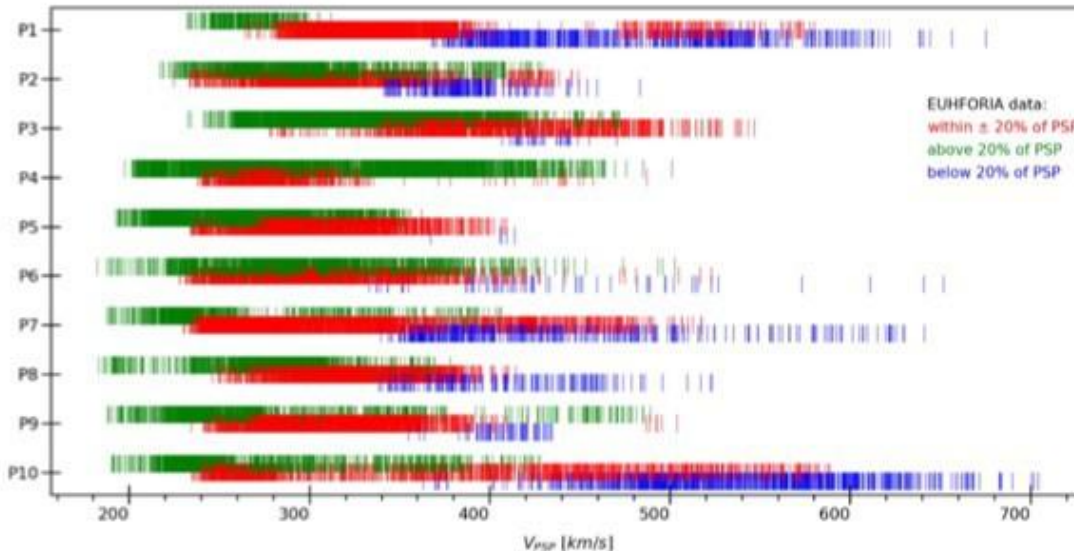


Figure 6. The accuracy of the solar wind modelling with EUHFORIA for the first 10 PSP close encounters. The dominance of the green coloured regions which represent the solar wind velocity larger than the ambient PSP velocity increased for the 20% of its value indicates that the solar wind modelled by EUHFORIA is generally overestimated at the close to the Sun distances. This result is opposite to the one obtained by Hintereitter et al., (2019), for the close to Earth distances.

4.2 Modelling CMEs and the background solar wind with EUHFORIA

Modelling of CMEs is very strongly depending on the accurate modelling of the ambient solar wind. Here we present several publications in which studies of the modelling CMEs with the optimized background solar wind in EUHFORIA were performed.

4.2.1 Toroidal modified Miller-Turner CME model in EUHFORIA: Validation and comparison with flux rope and spheromak

This work was presented in the publication: Maharana, A., Linan, L., Poedts, S. et al., 2024, *Astronomy & Astrophysics*.

In this study, we demonstrate the application of the modified Miller-Turner (mMT) model implemented within EUHFORIA in forecasting the geo-effectiveness of CME events in the heliosphere. Our goal is to develop a model that not only has a global geometry, in order to improve overall forecasting, but is also fast enough for operational space-weather forecasting. We test the original full torus implementation and introduce a new three-fourths Torus version called the Horseshoe CME model (Fig.7). This new model has a more realistic CME geometry and overcomes the inaccuracies of the full torus geometry. We constrain the torus geometrical and magnetic field parameters using observed signatures of the CMEs before, during, and after the eruption. We perform EUHFORIA simulations for two validation cases – the isolated CME event of 12 July 2012 and the CME–CME interaction event of 8–10

September 2014. We performed an assessment of the model's capability to predict the most important B_z component using the advanced dynamic time-warping technique. The Horseshoe model predictions of CME arrival time and geo-effectiveness for both validation events compare well with the observations and are weighed against the results obtained with the spheromak and FRI3D models, which were already available in EUHFORIA. The runtime of the Horseshoe model simulations is close to that of the spheromak model, which is suitable for operational space weather forecasting. However, the capability of the magnetic field prediction at 1 au of the Horseshoe model is close to that of the FRI3D model. In addition, we demonstrate that the Horseshoe CME model can be used for simulating successive CMEs in EUHFORIA, overcoming a limitation of the FRI3D model.

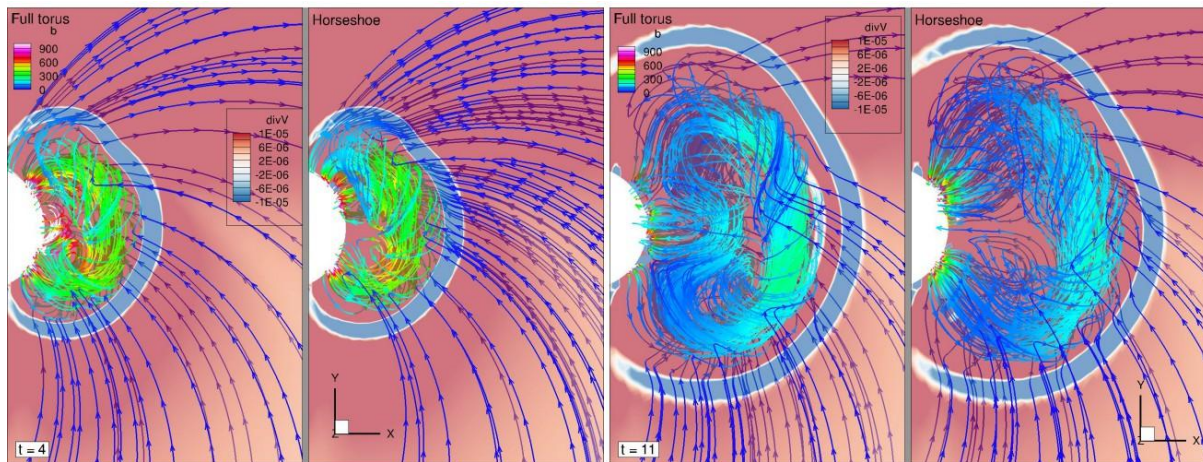


Figure 7. Equatorial snapshot of EUHFORIA simulations of the full torus and the Horseshoe implementation of the mMT magnetic field configuration. The evolution of the internal magnetic field lines of the CMEs (colour-coded with the magnetic field strength), 4 hours (panels 1–2), and 11 hours (panels 3–4), respectively, after the start of the injection at 0.1 au, is illustrated. In the background, the divergence of the speed is plotted. The sheath ahead of the magnetic cloud is depicted by the negative divergence (accumulation of plasma) region, showing a clear envelope around the CME. In panels 1 and 3, the rear part of the full torus is seen injected, whereas panels 2 and 4 show the horseshoe-like geometry creating CME leg-like structures connected to the inner boundary

4.2.2 Employing the Coupled EUHFORIA – OpenGGCM model to predict CME Geoeffectiveness

This work was presented in the publication: Maharana, A., Cramer, W. D., Samara, E. et al., 2024, Space Weather.

Although EUHFORIA can predict the solar wind plasma and magnetic field properties at Earth, it is not equipped to quantify the geo-effectiveness of the solar transients in terms of geomagnetic indices like the disturbance storm time (Dst) index and the auroral indices, that quantify the impact of the magnetized plasma encounters on Earth's magnetosphere. Therefore, we couple EUHFORIA with the Open Geospace General Circulation Model (OpenGGCM), a magnetohydrodynamic model of the response of Earth's magnetosphere, ionosphere, and thermosphere to transient solar wind characteristics. In this coupling, OpenGGCM is driven by the solar wind and interplanetary magnetic field obtained from EUHFORIA simulations to produce the magnetospheric and ionospheric response to the CMEs. This coupling is validated with two observed geo-effective CME events driven with the spheromak flux-rope CME model.

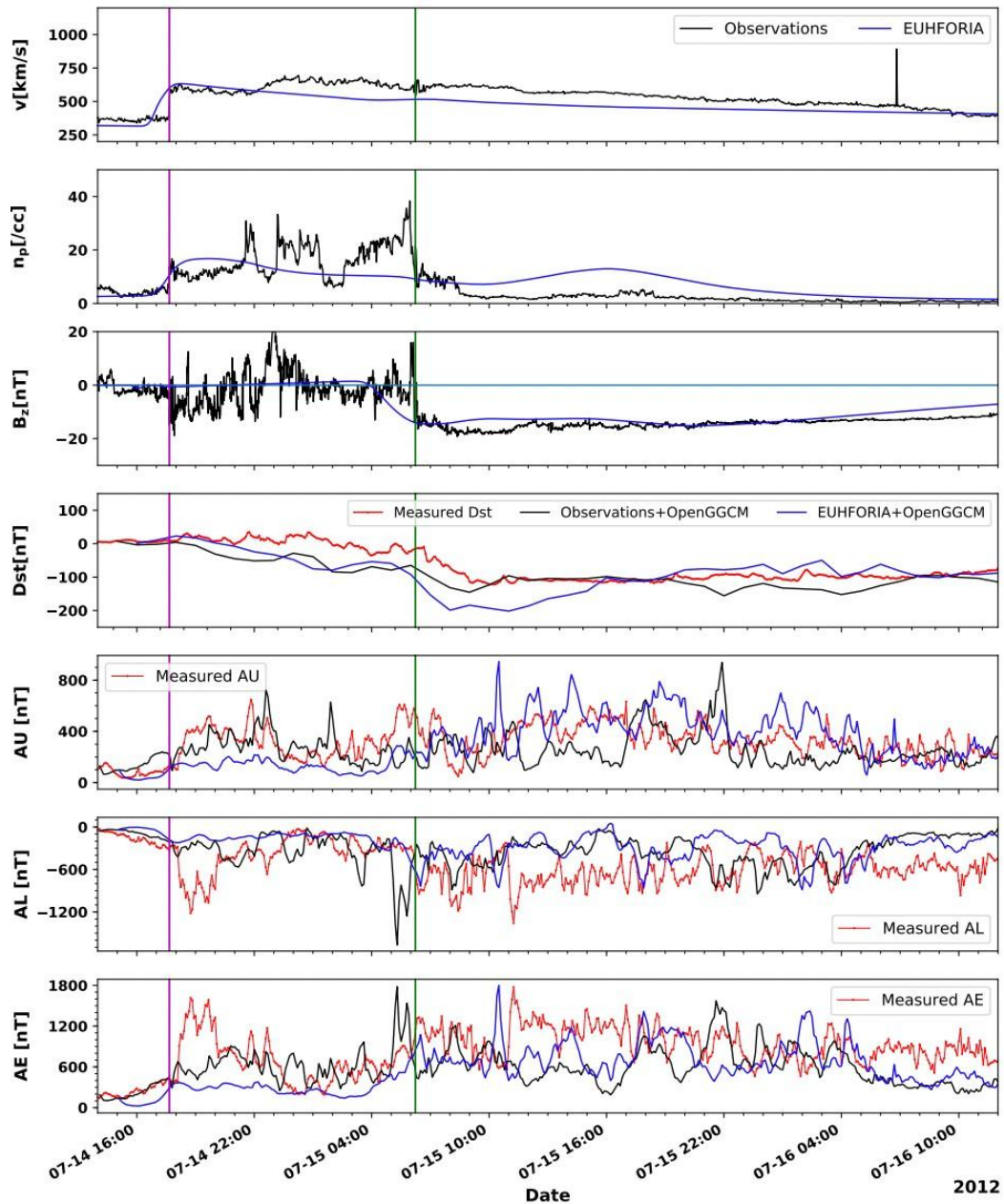


Figure 8. Characteristics and predicted geomagnetic indices of Event 1. Panels 1-3 show the plasma parameters – speed (v), proton number density (n_p), and the magnetic field parameter – z-component of magnetic field (B_z) as obtained from the Wind spacecraft in situ observations (in black) and the EUHFORIA simulation of the event based on modified Scolini et al. (2019) (in blue), respectively. The horizontal blue line in Panel 3 corresponds to $B_z = 0$. Panels 4–7 show the geomagnetic indices – Dst index, AU index, AL index, and AE index as measured in Earth’s magnetosphere and ionosphere (in red), and as obtained from OpenGGCM simulations using input from the Wind (in black) and EUHFORIA simulation (in blue). The magenta and green vertical solid lines depict the arrival of the CME shock and the beginning of the magnetic cloud passage at Earth, respectively.

We compare these simulation results with the indices obtained from OpenGGCM simulations driven by the measured solar wind data from spacecraft (Fig.8). We further employ

the dynamic time warping (DTW) technique to assess the model performance in predicting Dst. The main highlight of this study is to use EUHFORIA simulated time series to predict the Dst and auroral indices 1-2 days in advance, as compared to using the observed solar wind data at L1, which only provides predictions 1-2 hr before the actual impact.

4.2.3 Validation of EUHFORIA cone and spheromak coronal mass ejection models

This work was presented in the publication: Rodriguez, L., Warmuth, A., Andretta, V. et al., 2023, Solar Physics.

Our study focuses on validation of the estimation of the arrival times and geomagnetic impact of CMEs using the cone and spheromak CME models implemented in the EUHFORIA code. Validating numerical models is crucial for ensuring their accuracy and performance with respect to real data.

We compared CME plasma and magnetic field signatures measured in situ by satellites at the L1 point with the simulation output of EUHFORIA. The validation was carried out using two datasets in order to ensure a comprehensive evaluation. The first dataset focuses on 16 CMEs that arrived at Earth, offering specific insights into the model's accuracy in predicting arrival time and geomagnetic impact. Meanwhile, the second dataset encompasses all CMEs observed over eight months within Solar Cycle 24, regardless of whether or not they arrived at Earth, covering periods of both solar minimum and maximum activity. This second dataset enables a more comprehensive evaluation of the model's predictive precision in terms of CME arrivals and misses. Our results show that EUHFORIA provides good estimates in terms of arrival times, with root mean square error (RMSE) values of 9 hours. Regarding the number of correctly predicted ICME arrivals and misses, we find a 75% probability of detection in a 12h time window and 100% probability of detection in a 24 hour time window. The geomagnetic impact forecasts measured by the Kp index provide different degrees of accuracy ranging from 31% to 69%. These results validate the use of cone and spheromak CMEs for real-time space weather forecasting.

4.2.4 EUHFORIA modelling of the magnetic cloud on June 28, 2013

This work was presented in the publication: Prete, G., Niemela, A., Schmieder, B. et al., 2024, Astronomy & Astrophysics.

The aim of this study was to test accuracy of the EUHFORIA simulations in the chain of a series of CME events detected from L1 back to the Sun in order to determine the relationship between remote and in situ CMEs. We have analysed both remote-sensing observations and in situ measurements of a well-defined magnetic cloud (MC) detected at L1 occurring on 28 June 2013. After computing the background solar wind with EUHFORIA, we tested the trajectories of six CMEs occurring in a time window of five days before a well-defined MC at L1 that may act as the candidate of the MC. We modelled each CME using the cone model. The test involving all the CMEs indicated that the main driver of the well-defined, long-duration MC was a slow CME. For the corresponding MC, we retrieved the arrival time and the observed proton density.

Modelling results with EUHFORIA confirm the results obtained in the George Mason data catalogue concerning this chain of events. However, their proposed solar source of the CME is disputable. The slow CME at the origin of the MC could have its solar source in a small, emerging region at the border of a filament channel at latitude and longitude equal to +14 degrees.

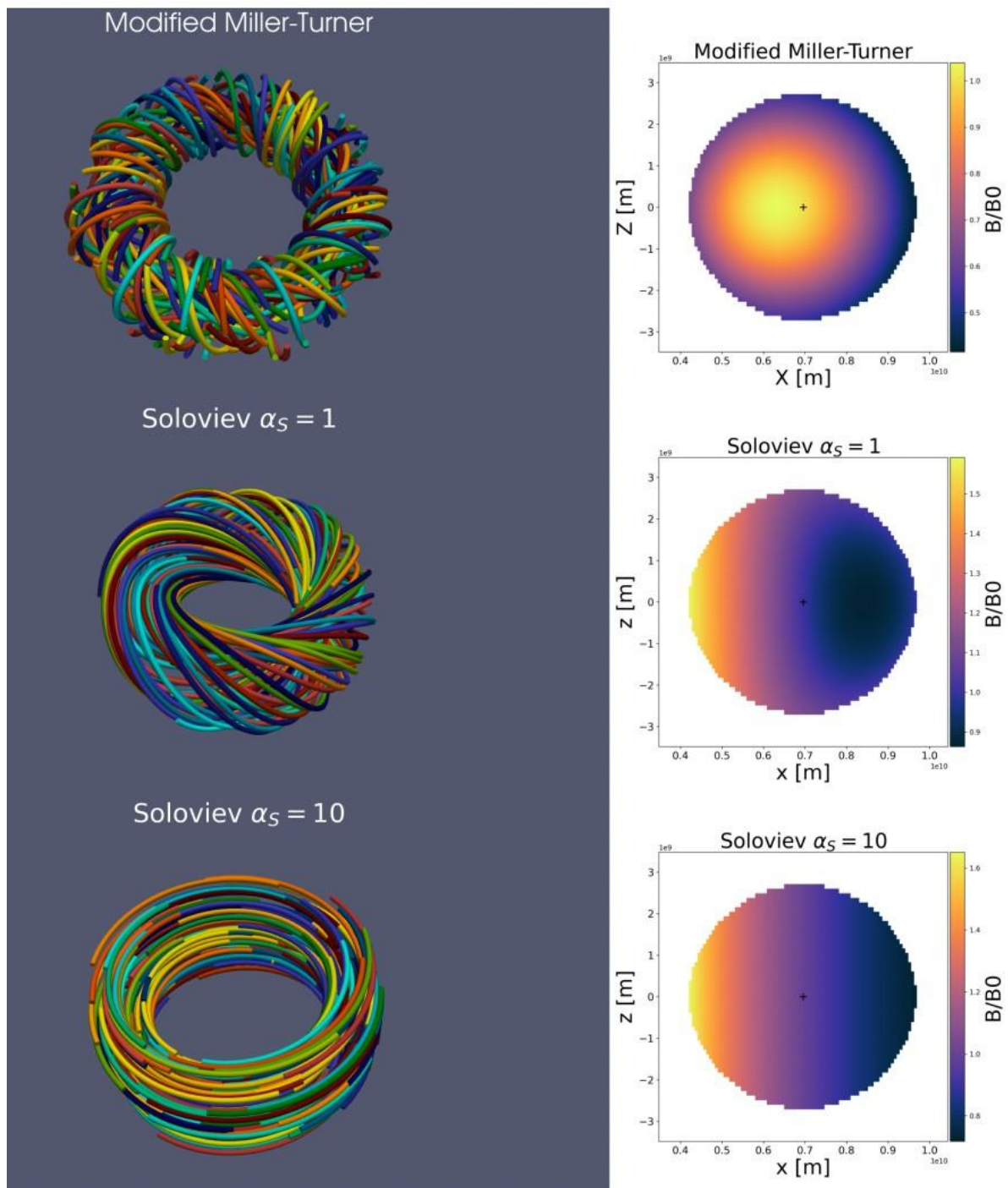


Figure 9. Normalized magnetic field strength in the two CME models implemented in EUHFORIA. The left panels show a sample of magnetic field lines in a torus with a minor radius $a = 4R_{\odot}$ and a major radius $R_M = 10 R_{\odot}$. The right panels show the dimensionless magnetic field strength B/B_0 in a poloidal cross-section. The “+” markers indicate the center of the torus. From top to bottom: magnetic field configuration in the modified Miller-Turner model, in the Soloviev model with $\alpha_S = 1$ and with $\alpha_S = 10$. When the α_S parameter is too high, the magnetic field is mainly toroidal.

4.2.5 Toroidal Miller-Turner and Soloviev CME models in EUHFORIA

This work was presented in the publication Linan, L., Maharana, A., Poedts, S. et al., 2024, *Astronomy & Astrophysics*.

The prediction capabilities by EUHFORIA are directly related to the geometric, thermodynamic, and magnetic properties of the injected CME models. The aim of this study is to present the implementation of two new CME models in EUHFORIA. Both models possess a toroidal geometry, but the internal distribution of the magnetic field is different. We introduce the two toroidal CME models analytically, along with their numerical implementation in EUHFORIA. One model is based on the modified Miller-Turner (mMT) solution, while the other is derived from the Soloviev equilibrium, a specific solution of the Grad-Shafranov equation. The magnetic field distribution in both models is provided in analytic formulae, enabling a swift numerical computation. After detailing the differences between the two models, we present a collection of thermodynamic and magnetic profiles obtained at Earth using these CME solutions in EUHFORIA with a realistic solar wind background. Subsequently, we explore the influence of their initial parameters on the time profiles at L1. In particular, we examine the impact of the initial density, magnetic field strength, velocity, and minor radius.

The Soloviev model allows control over the shape of the poloidal cross section, as well as the initial twist. In EUHFORIA, we obtained different thermodynamic and magnetic profiles depending on the CME model used. The generated magnetic profiles reflect the initial magnetic field distribution of the chosen model. We found that changing the initial parameters affects both the amplitude and the trend of the time profiles. For example, using a high initial speed results in a fast evolving and compressed magnetic structure. The speed of the CME is also linked to the strength of the initial magnetic field due to the contribution of the Lorentz force on the CME expansion. However, increasing the initial magnetic field also increases the computation time. Finally, the expansion and integrity of the magnetic structure can be controlled via the initial density of the CME.

We conclude that both toroidal CME models are successfully implemented in EUHFORIA and can be utilized to predict the geo-effectiveness of the impact of real CME events. Moreover, the current implementation could be easily modified to model other toroidal magnetic configurations.

4.3 Modeling solar energetic particles (SEPs) accelerated at the CME-driven shocks in the background solar wind of EUHFORIA

In the framework of the SWiM project we have also performed few studies focused on modelling of solar energetic particle (SEP) events. This subsection provides a brief overview.

4.3.1 Advancing interplanetary magnetohydrodynamic models through solar energetic particle modelling. Insights from the 2013 March 15 SEP event

This work was presented in the publication: Niemela, A., Wijsen, N., Aran, A. et al., 2023, *Astronomy & Astrophysics*.

This study utilises a modelling approach to investigate the impact of perturbed solar wind conditions caused by multiple ICMEs on the evolution of SEPs distributions. Furthermore, we demonstrate the utility of SEP models in evaluating the performance of solar wind and CME models.

To illustrate these concepts, we focussed on modelling the gradual SEP event that occurred on 2023 March 15 (see Fig.10).

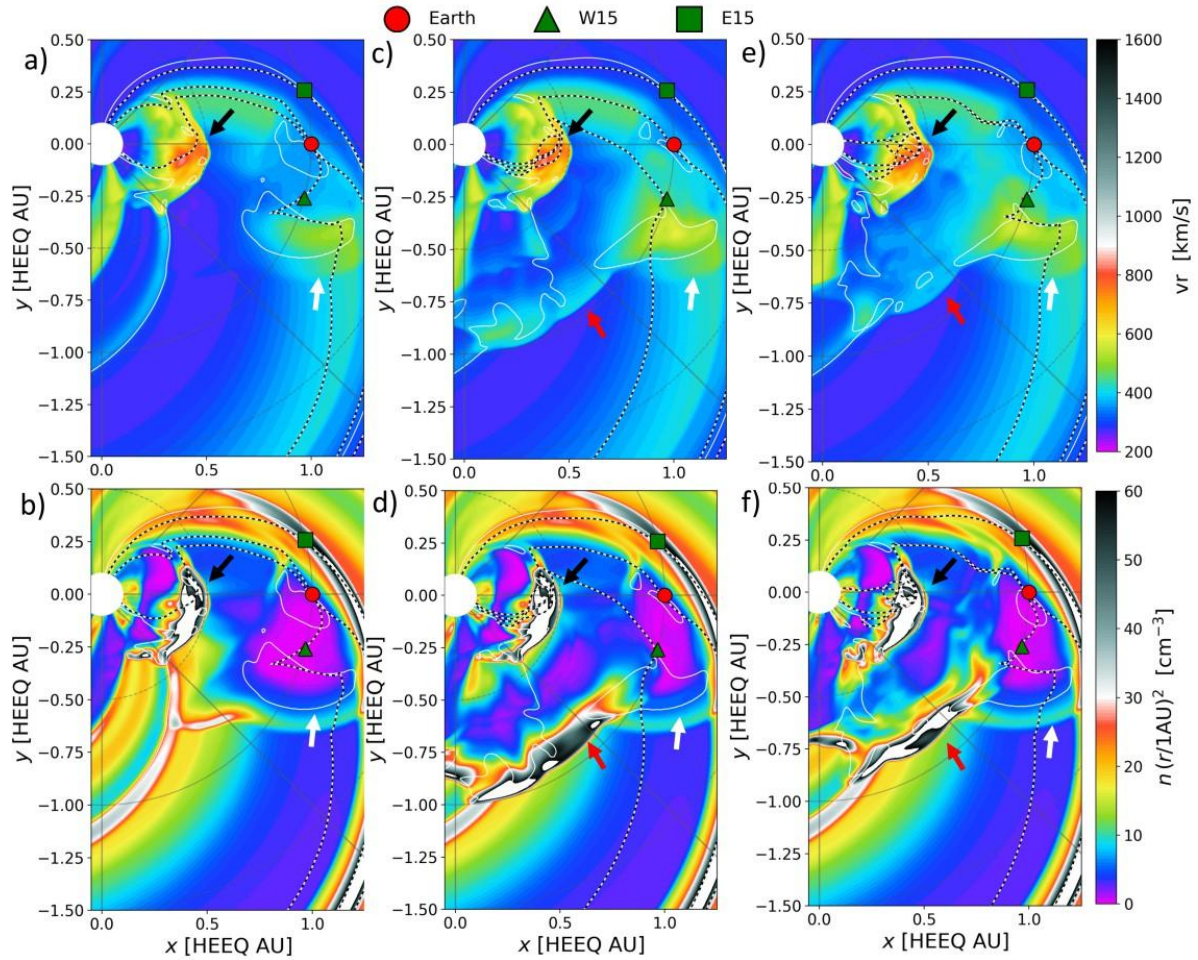


Figure 10. Snapshot of the EUHFORIA simulations for Case 1 (a and b), Case 2 (c and d), and Case 3 (e and f) for 2013 March 16 at 06:44 UT. The top row shows the radial solar wind speed, and the bottom row shows the scaled number density in the equatorial plane. White, red, and black arrows point at the approximate position of the First, Second, and Main CMEs (respectively). Dashed lines correspond to the magnetic field line connection from the E15, Earth, and W15 positions, backtracked to 0.1 au.

We employed EUHFORIA to simulate the several ICMEs that induced the highly perturbed solar wind conditions observed during the March 15 event. We conducted three separate EUHFORIA simulations, employing both non-magnetised and magnetised models for these ICMEs. To analyse the behaviour of energetic particles in the simulated solar wind environments, we employed the energetic particle transport and acceleration model PARADISE (PARTicle Radiation Asset Directed at Interplanetary Space Exploration). We have found that in the vicinity of Earth, the three EUHFORIA simulations exhibit strong similarities and closely match the observed in situ data. Nevertheless, when incorporating these distinct solar wind configurations into PARADISE, notable disparities emerge in the simulated SEP intensities. This discrepancy can be attributed to the different magnetic enhancements and closed magnetic structures introduced by the different CME models within the EUHFORIA simulations. These variations strongly impact the transport mechanisms of SEPs, leading to significant deviations in the particle intensities simulated by PARADISE.

Furthermore, our findings highlight the significance of cross-field diffusion even in scenarios with reduced perpendicular mean free path. This effect becomes particularly prominent when SEPs are trapped within the inner heliosphere due to the presence of ICMEs. In these scenarios, the extended duration of confinement allows the slower cross-field diffusion process to become more pronounced and exert a greater influence on the spatial distribution of SEPs, especially near and within the boundaries of ICMEs.

More generally, solar energetic particle models enable us to indirectly validate the accuracy of the underlying solar wind and CME models across significant portions of the heliosphere, rather than solely relying on discrete points where spacecraft are situated. This broader validation provides valuable insights into the reliability and effectiveness of the CME models on a global scale.

4.3.2 Cannibals in PARADISE: The Effect of Merging Interplanetary Shocks on Solar Energetic Particle Events

This work was presented in the publication: Niemela, A., Wijsen, N., Aran, A. et al., 2024, *The Astrophysical Journal Letters*.

Gradual SEP events are associated with shocks driven by CMEs. The merging of two CMEs (so-called cannibalistic CMEs) and the interaction of their associated shocks has been linked to some of the most powerful solar storms ever recorded. Multiple studies have focused on the observational aspects of these SEP events, yet only a handful have focused on modelling similar CME–CME interactions in the heliosphere using advanced MHD models. This work presents, to our knowledge, the first modelling results of a fully time-dependent 3D simulation that captures both the interaction of two CMEs and its effect on the acceleration and transport of SEPs. This is achieved by using an MHD model for the solar wind and CME propagation together with an integrated SEP model. We perform different simulations and compare the behaviour of the energetic protons in three different solar wind environments, where a combination of two SEP-accelerating CMEs. We find that particle acceleration is significantly affected by the presence of both CMEs in the simulation. Initially, less efficient acceleration results in lower-energy particles. However, as the CMEs converge and their shocks eventually merge, particle acceleration is significantly enhanced through multiple acceleration processes between CME-driven shocks, resulting in higher particle intensities and energy levels.

4.3.3 Modelling two energetic storm particle events observed by Solar Orbiter using the combined EUHFORIA and iPATH models

This work was presented in the publication: Ding, Z., Li, G., Mason, G. et al., 2024, *Astronomy & Astrophysics*.

The main focus is on modelling two energetic storm particle events observed by Solar Orbiter using the combined EUHFORIA and iPATH models. We have coupled EUHFORIA and the improved Particle Acceleration and Transport in the Heliosphere (iPATH) models. Further, we modelled two energetic storm particle (ESP) events originating from the same active region AR 13088, and observed by Solar Orbiter on August 31, 2022, and September 5, 2022. Aim of the study is to combine numerical simulations and Solar Orbiter observations, in order to better understand particle acceleration and the transport process in the inner heliosphere.

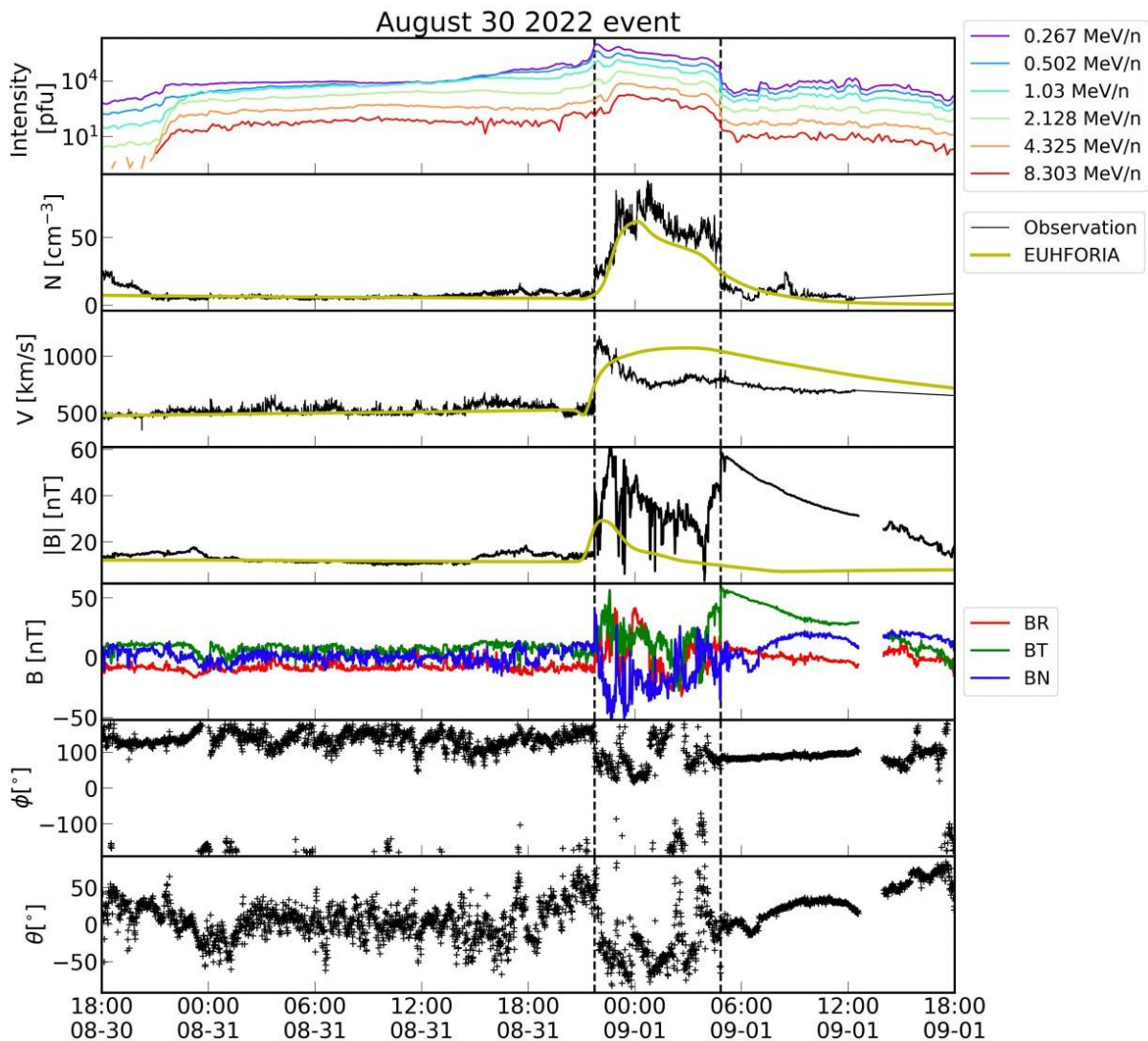


Figure 11. SEP time profiles and in situ plasma and magnetic field for the August 30, 2022 event. The panels present, from top to bottom, the energetic proton time profiles, the solar wind proton number density, the solar wind speed, the magnetic field magnitude, the magnetic field vector measured in the RTN coordinate system, and azimuthal (ϕ) and elevation (θ) angles of the unit vector magnetic field. The yellow lines represent the EUHFORIA simulation results. The dashed lines indicate the IP shock and the end of the ESP event.

We simulated two CMEs in a data-driven, real-time solar wind background with the EUHFORIA code. The MHD parameters concerning the shock and downstream medium were computed from EUHFORIA as inputs for the iPATH model. In the iPATH model, a shell structure was maintained to model the turbulence-enhanced shock sheath. At the shock front, assuming diffuse shock acceleration, the particle distribution was obtained by taking the steady state solution with the instantaneous shock parameters. Upstream of the shock, particles escape, and their transport in the solar wind was described by a focused transport equation using the backward stochastic differential equation method. Although both events originated from the same active region, they exhibited notable differences. One such difference is the duration of the events, as the August ESP event lasted for 7h (Fig.11), while

the September event persisted for 16h. Another key difference concerns the time intensity profiles. The September event showed a clear crossover upstream of the shock where the intensity of higher energy protons exceeds those of lower energy protons, leading to positive ("reverse") spectral indices prior to the shock passage. For both events, our simulations replicate the observed duration of the shock sheath, depending on the deceleration history of the CME. Imposing different choices of escaping length scale, which is related to the decay of upstream turbulence, the modelled time intensity profiles prior to the shock arrival also agree with observations. In particular, the crossover of this time profile in the September event is well reproduced. We show that a "reverse" upstream spectrum is the result of the interplay between two length scales. One characterizes the decay of the accelerated particles upstream of the shock, which are controlled by the energy-dependent diffusion coefficient, and the other characterizes the decay of upstream turbulence power, which is related to the process of how streaming protons upstream of the shock excite Alfvén waves.

We concluded that the behavior of the SEP events depends on many variables. Even similar eruptions from the same AR may lead to SEP events that have very different characteristics. Simulations taking into account real-time background solar wind, the dynamics of the CME propagation, and upstream turbulence at the shock front are necessary to thoroughly understand the ESP phase of large SEP events.

4.4 COCONUT - new coronal model for EUHFORIA and wider

The new coronal model COCONUT was developed and described in several publications, some of them presented here.

4.4.1 COCONUT, a Novel Fast-converging MHD Model for Solar Corona Simulations: I. Benchmarking and Optimization of Polytopic Solutions

This work was presented in the publication: Perri, B., Leitner, P., Brchnelova, M. et al., 2022, The Astrophysical Journal.

In this publication we present a novel global 3D coronal MHD model called COCONUT, polytropic in its first stage and based on a time-implicit backward Euler scheme. Our model boosts run-time performance in comparison with contemporary MHD-solvers based on explicit schemes, which is particularly important when later employed in an operational setting for space-weather forecasting. It is data-driven in the sense that we use synoptic maps as inner boundary inputs for our potential-field initialization as well as an inner boundary condition in the further MHD time evolution. The coronal model is developed as part of the EUHFORIA and it is aimed to replace the currently employed, more simplistic, empirical WSA model. At 21.5 Ro where the solar wind is already supersonic, it is coupled to EUHFORIA's heliospheric model. We validate and benchmark our coronal simulation results with the explicit-scheme Wind-Predict model and find good agreement for idealized limit cases as well as real magnetograms, while obtaining a computational time reduction of up to a factor 3 for simple idealized cases, and up to 35 for realistic configurations, and we demonstrate that the time gained increases with the spatial resolution of the input synoptic map. We also use observations to constrain the model and show that it recovers relevant features such as the position and shape of the streamers (by comparison with eclipse white-light images), the coronal holes (by comparison with EUV images), and the current sheet (by comparison with WSA model at 0.1 au).

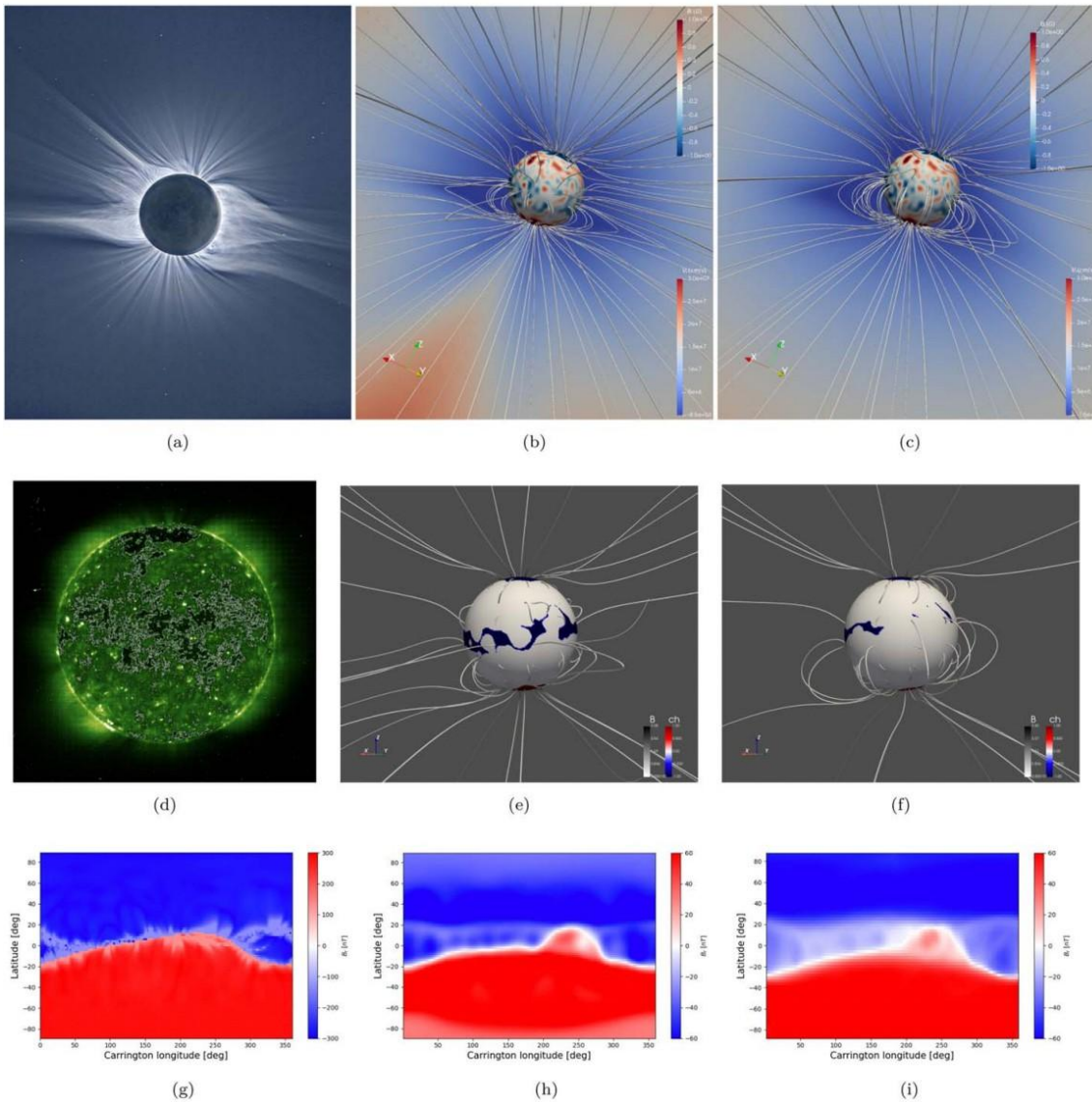


Figure 12. Comparison with observations for the case $l_{\max} = 30$ for the GONG synoptic map of 2008 August 1. The first column presents the observations of that day in white light (a), EUV (d), and the WSA model at 0.1 au. The second column (panels (b), (e), and (h)) shows the corresponding results for COCONUT. The third column (panels (c), (f), and (i)) shows the corresponding results for Wind-Predict. Panels (g), (h) and (i) show the comparison for 2008 August 1 GONG synoptic map case for the boundary conditions at 0.1 au between the: WSA solution, the COCONUT solution, and the Wind-Predict solution with its usual boundary conditions, respectively. The radial magnetic field B_r is in nT.

4.4.2 COCONUT, a Novel Fast-converging MHD Model for Solar Corona Simulations. II. Assessing the Impact of the Input Magnetic Map on Space-weather Forecasting at Minimum of Activity

This work was presented in the publication: Perri, B., Kuźma, B., Brchnelova, M. et al., 2023, The Astrophysical Journal.

The study is focused to the new implicit unstructured coronal code COCONUT, which aims at providing fast and accurate inputs for space-weather forecasting as an alternative to

empirical models. We use all 20 available magnetic maps of the solar photosphere covering the date of 2019 July 2, which corresponds to a solar eclipse on Earth. We use the same standard preprocessing on all maps, then perform coronal MHD simulations with the same numerical and physical parameters. In the second step we are quantifying the performance of each map using three indicators from remote-sensing observations: white-light total solar eclipse images for the streamers' edges, EUV synoptic maps for coronal holes, and white-light coronagraph images for the heliospheric current sheet (Fig. 13). We found that the model performance is between 24% and 85% for the streamers' edges, 24%-88% for the coronal hole boundaries, and a mean deviation between 4° and 12° for the heliospheric current sheet position. We find that the HMI runs perform better on all indicators, with GONG-ADAPT being the second-best choice. HMI runs perform better for the streamers' edges, and GONG-ADAPT for polar coronal holes, HMI synchronic for equatorial coronal holes, and the streamer belt. We especially illustrate the importance of the filling of the poles. This demonstrates that the solar poles have to be taken into account even for ecliptic plane previsions.

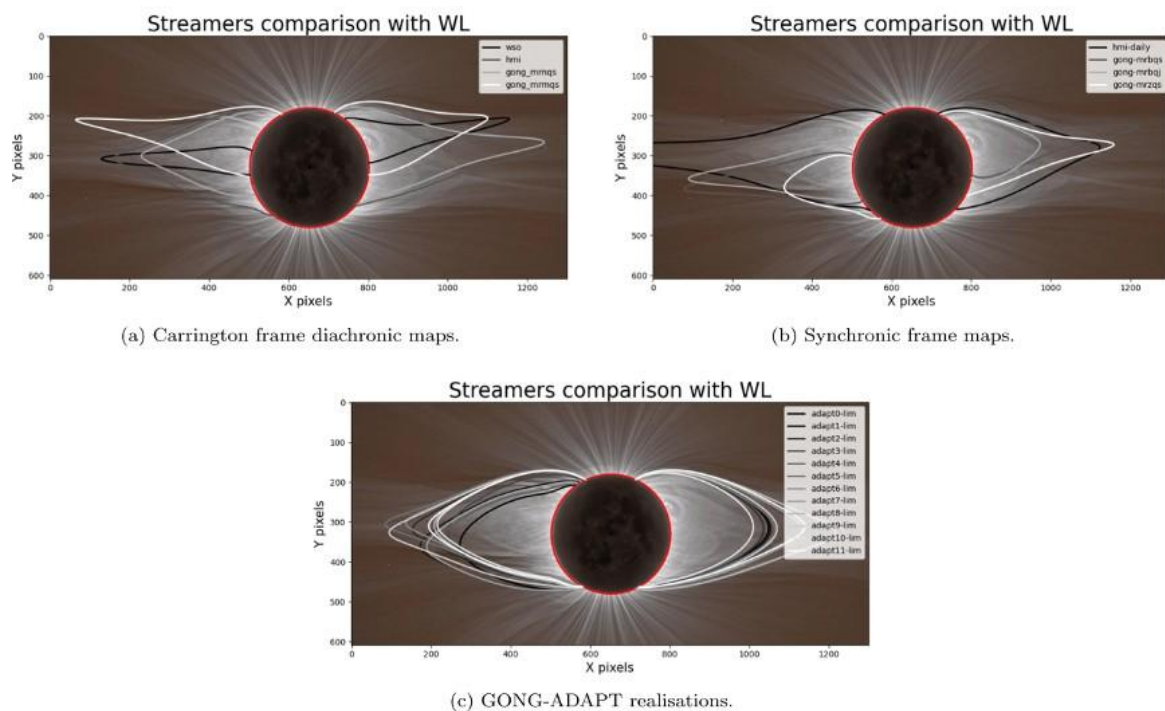


Figure 13. Comparison of the shape of the meridional streamers with the white-light eclipse image from 2019 July 2. The first panel compares the streamers from Carrington frame diachronic maps, the second from synchronic frame maps, and the last one from all 12 GONG-ADAPT realisations. The solar disk is highlighted as a red circle as reference. Streamer contours are shown as gray shades. All streamers have been remapped to the same size ratio using this reference and its conversion to the picture pixels, shown as an axis.

4.4.3 COCONUT-MF: Two-fluid ion-neutral global coronal modelling

This work was presented in the publication: Brchnełova, M., Kuźma, B., Zhang, F. et al., 2023, *Astronomy & Astrophysics*.

The global coronal model COCONUT (COolfluid COronal uNstrUcTured) was originally developed to replace semiempirical models such as the Wang-Sheeley-Arge model in space weather forecasting chains to improve the physical accuracy of the predictions. This model has, however, several simplifications implemented in its formulation to allow for rapid convergence in an operational setting. These simplifications include the assumptions that the

plasma is fully ionised, sufficiently collisional, and that quasi-neutrality holds, so that it can be modelled as a single fluid. This means that all interactions with the low-concentration neutral fluid in the corona, such as collisions or charge exchange, are neglected.

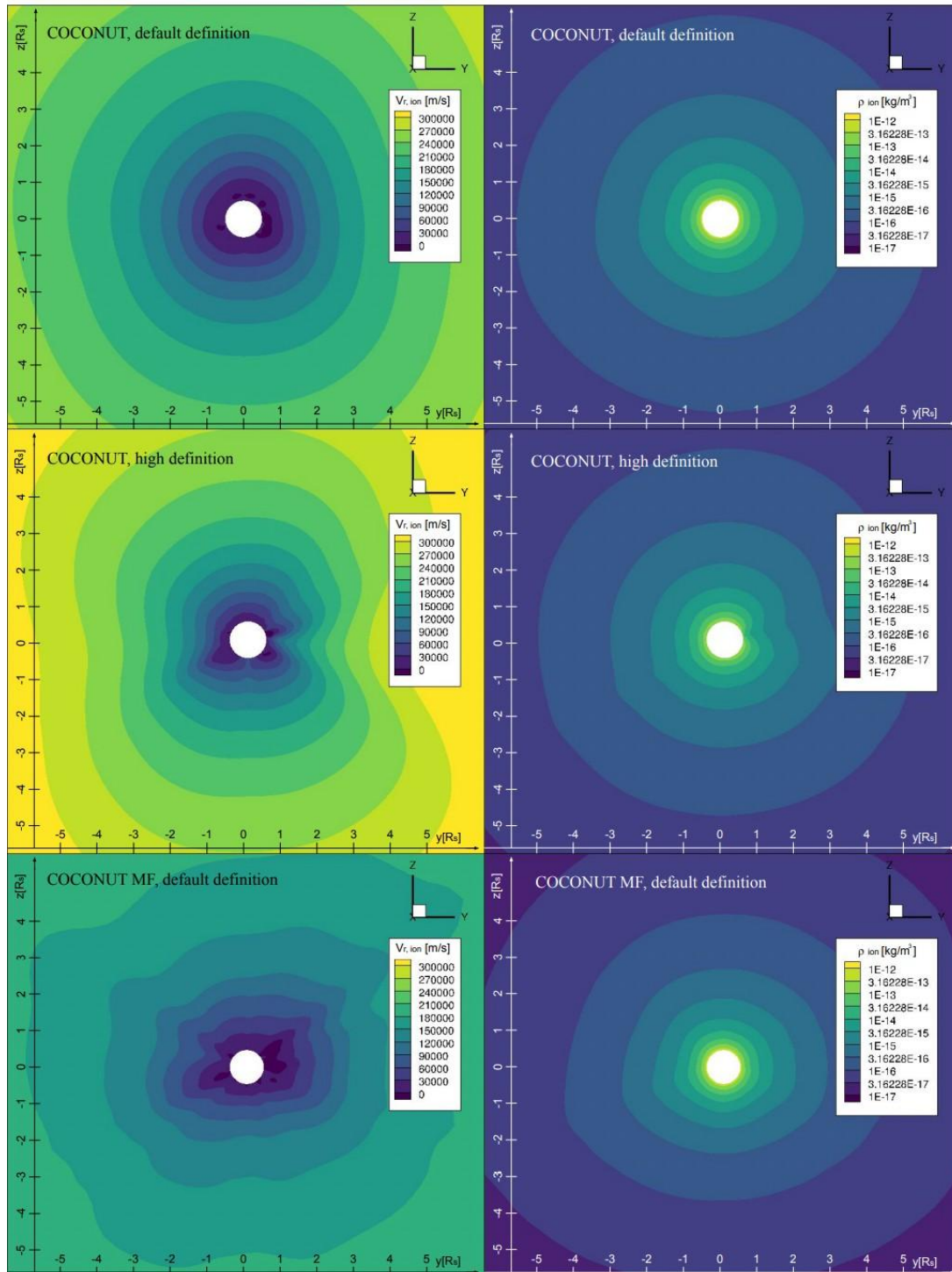


Figure 14. Comparison between the ideal MHD and MFMHD simulations of the solar maximum case. The top row shows the ideal MHD case at the same grid resolution as the MFMHD case in the bottom row. Since this solution is more dissipated due to the different scheme, a higher resolution, lower-dissipation ideal MHD solution is shown in the middle to confirm the correct positioning of the streamers resolved in the MFMHD result. The left panels show the ion radial velocity and the right panels the ion density profiles.

In this study we have focused to two goals. Firstly, we aim to introduce a novel multi-fluid global coronal model and validate it with simple cases (like a magnetic dipole) as well as with real data-driven applications. Secondly, we aim to investigate to what extent considering a single-fluid plasma in the global coronal model might affect the resulting plasma dynamics, and thus whether the assumptions on which the single-fluid coronal model is based are justified. We have developed a multi-fluid global coronal model following the ideal MHD COCONUT model, COCONUT-MF, which resolves the ion and neutral fluid equations separately. While this model is still steady-state and thus does not resolve unsteady processes, it can account for resistivity, charge exchange, and chemical (ionisation and recombination) and collisional contributions due to the presence of the neutrals in the fluid equations. We present the results of the ion-neutral COCONUT-MF modelling for a magnetic dipole, a minimum of solar activity case (August 1, 2008), and a solar maximum case (March 9, 2016). Through comparison with the ideal MHD results, we confirm that the resolved multi-fluid solver features are physical and also demonstrate the higher accuracy of the applied upwind numerical flux scheme compared to the one used in the original MHD model. Subsequently, we also repeat the multi-fluid simulations while excluding the charge exchange and the chemical and collisional terms to evaluate the effect these terms have on the resulting plasma dynamics. It is observed in numerical results that, despite the very low concentration of neutrals, they still do affect the flow field to a limited but non-negligible extent (up to 5 to 10% locally), with a higher impact being seen in the case of the solar maximum. It is also demonstrated that the collisional terms are primarily responsible for the neutrals adopting the electromagnetic profiles of the ions, while the charge exchange and chemical terms yield the largest thermal effects of the neutrals on the ion plasma. Despite the fact that the coronal plasma is generally assumed to be collisionless, our results show that there is sufficient collisionality in it to couple the two fluids.

4.4.4 Numerical Nuances of Global Coronal Models

This work was presented in the publication: Brchnelova, M., Kuźma, B., Perri, B. et al., 2022, The Astrophysical Journal Supplement Series.

During recent years, global coronal models have experienced an ongoing increase in popularity as tools for forecasting solar weather. Within the domain of up to 0,1 au, MHD is used to resolve the coronal structure using magnetograms as inputs at the solar surface. Ideally, these computations would be repeated with every update of the solar magnetogram so that they could be used in the ESA Modeling and Data Analysis Working Group magnetic connectivity tool (<http://connect-tool.irap.omp.eu/>). Thus, it is crucial that these results are both accurate and efficient. While much work has been published showing the results of these models in comparison with observations, not much of it discusses the intricate numerical adjustments required to achieve these results. These range from the details of boundary condition formulations to adjustments as large as enforcing parallelism between the magnetic field and velocity. By omitting the electric field in ideal MHD, the description of the physics can be insufficient and may lead to excessive diffusion and incorrect profiles. We formulate inner boundary conditions that, along with other techniques, reduce artificial electric field generation. Moreover, we investigate how different outer boundary condition formulations and grid design affect the results and convergence, with special focus on the density and radial component of the B -field. The significant improvement in accuracy of real magnetic map-driven simulations is illustrated for an example of the 2008 eclipse (Fig.15).

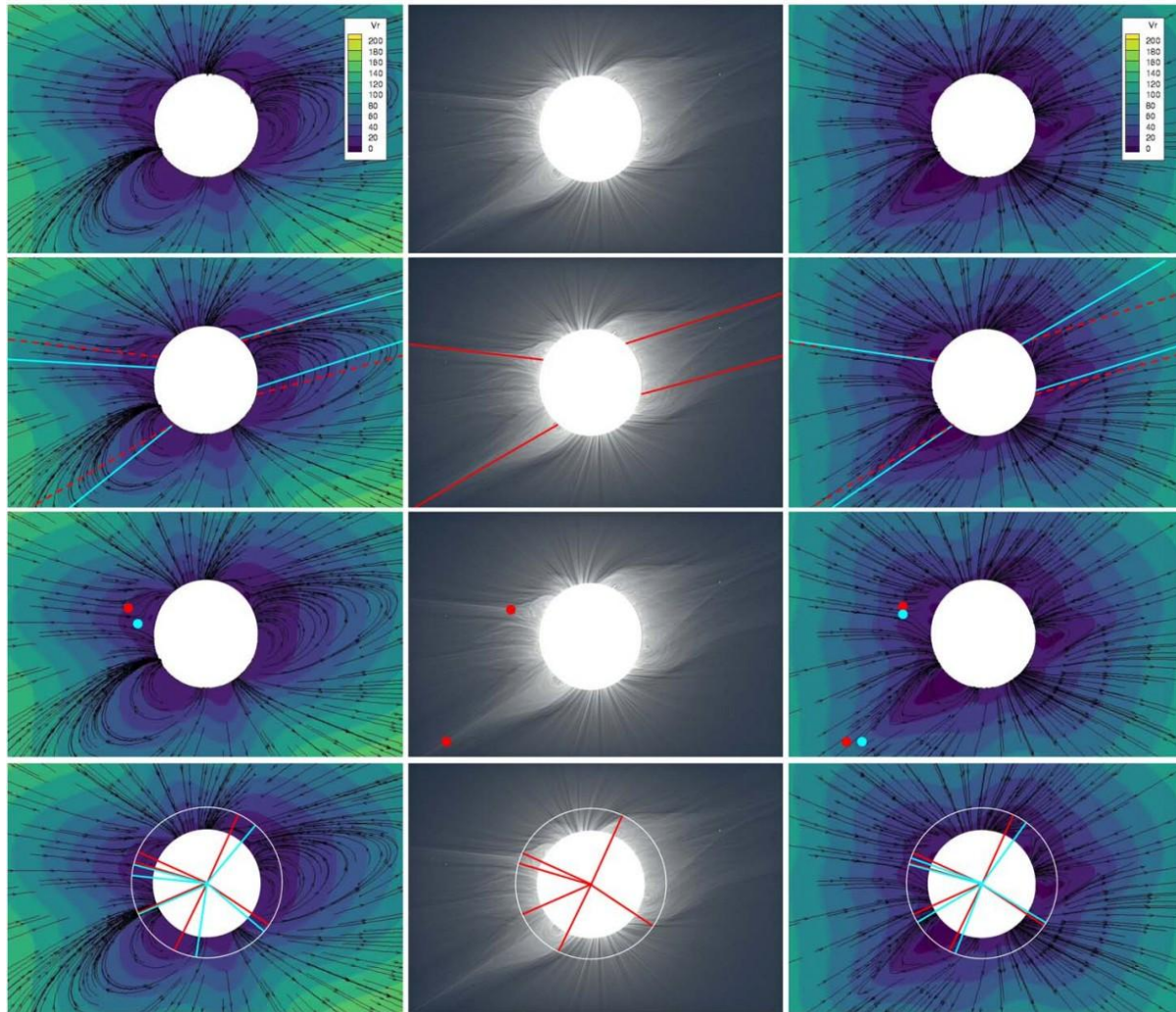


Figure 15. Comparison of the results of the 2008 simulation with “low E” (right) and “large E” (left) setups with the observations using the framework by Wagner et al. (2022).

4.4.5 Assessing inner boundary conditions for global coronal modeling of solar maxima

This work was presented in the publication: Brchneľova, M., Kuřma, B., Zhang, F. et al., 2023, Sun and Geosphere.

Computational Fluid Dynamics (CFD)-based global solar coronal simulations are slowly making their way into the space weather modelling tool-chains to replace the semi-empirical methods such as the WSA model. However, since they are based on CFD, if the assumptions in them are too strong, these codes might experience issues with convergence and unphysical solutions. Particularly the magnetograms corresponding to solar maxima can pose problems as they contain active regions with strong magnetic fields, resulting in large gradients. Combined with the approximate way in which the inner boundary is often treated, this can lead to non-physical features or even a complete divergence of the simulation in these cases. Herein, we show some of the possible approaches to handle this inner boundary in our global coronal model COCONUT in a way that improves both convergence and accuracy. Since we know that prescribing the photospheric magnetic field for a region that represents the lower corona is not entirely physical, first, we look at the ways in which we can adjust the input magnetograms to remove the highest magnitudes and gradients. Secondly, since in the

default setup we also assume a constant density, here we experiment with changing these values locally and globally to see the effect on the results. We conclude, through comparison with observations and convergence analysis, that modifying the density locally in active regions is the best way to improve the performance both in terms of convergence and physical accuracy from the tested approaches.

4.4.6 Constraining the inner boundaries of COCONUT through plasma β and Alfvén speed

This work was presented in the publication: Brchnelova, M., Gudiksen, B., Carlsson, M. et al., 2025, *Astronomy & Astrophysics*.

Global corona models require accurate boundary conditions, for the formulations of which we have very limited observational data. Unsuitable boundary condition prescriptions may lead to inconsistent features in the solution flow field and spoil the code's accuracy and performance. Aims. In this study we develop an adjustment to the inner boundary condition of the COCONUT global corona model to better capture the dynamics over and around the regions of stronger magnetic fields by constraining the plasma β and the Alfvén speed (Fig.16).

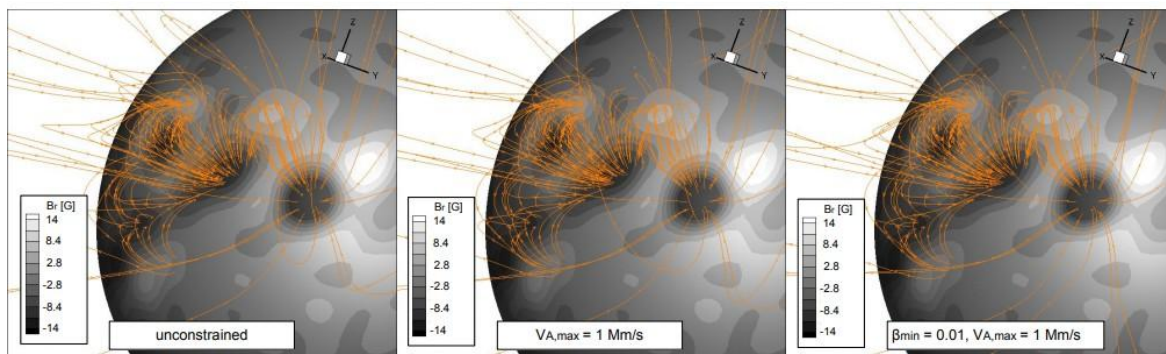


Figure 16. For the March 9, 2016 solar eclipse (CR2174), the detailed magnetic field lines are plotted over and around the strong active region causing the inexplicable high-speed streams for three levels of constraining (effectively no constraining on the left, $v_{A,max} = 10^6$ m/s in the middle and $v_{A,max} = 10^6$ m/s with $\beta_{min} = 10^{-2}$ constraining on the right).

Using data from solar observations and solar atmospheric modelling codes such as Bifrost, we find that the baseline homogeneous boundary condition formulations for pressure and density do not capture the plasma conditions physically accurately. We develop a method to adjust these prescribed pressure and density values by placing constraints on the plasma β and the Alfvén speed that act as proxies. We have demonstrated that we can remove inexplicable fast streams from the solution by constraining the maximum Alfvén speed and the minimum plasma β on the boundary surface. We also show that the magnetic topology is not significantly affected by this treatment otherwise. This technique shows the potential to ease the modelling of solar maxima, especially removing inexplicable features while, at the same time, not significantly affecting the magnetic field topology around the affected regions.

4.4.7 Magnetic connectivity from the Sun to the Earth with MHD models: I. Impact of the magnetic modelling on connectivity validation

This work was presented in the publication: Kennis, S., Perri, B., Poedts, S., 2024, *Astronomy & Astrophysics*.

The magnetic connectivity between the Sun and the Earth is crucial to our understanding of the solar wind and space weather events. However, establishing this connectivity is challenging because of the lack of direct observations, which explains the need for reliable simulations. The method most often used to make such measurements over the last few years is the two-step ballistic method, but it has many free parameters that can affect the final result. Thus, we want to provide a connectivity method based on self-consistent MHD models.

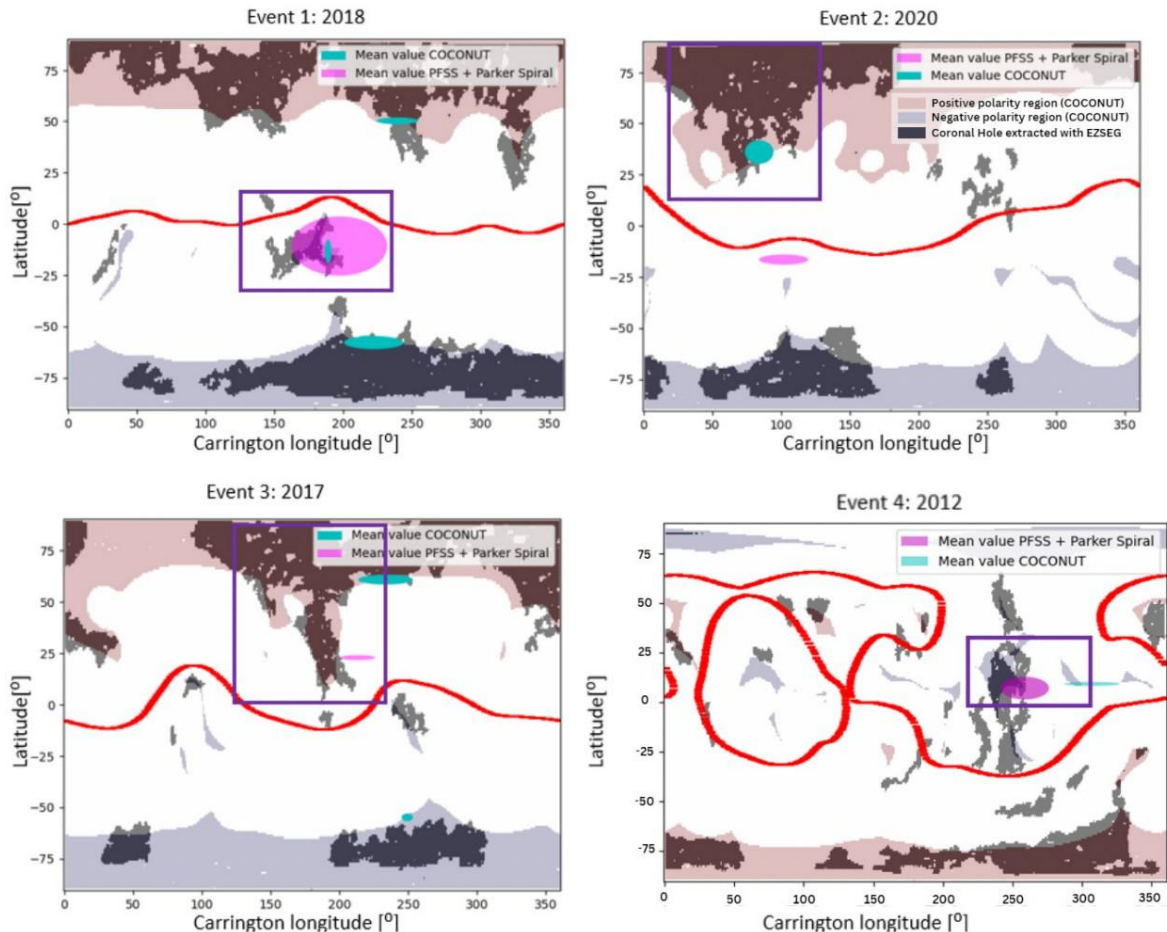


Figure 17. Validation of the MHD connectivity estimation for the four cases selected. We show the location at the surface of the Sun that is most likely to be connected to Earth during the corresponding HSS event. The MHD connectivity estimate is shown in bright blue, the two-step ballistic estimate is shown in pink, and the magnetic connectivity estimate from other studies (Reiss et al. 2021 for event 1 and Koukras et al. 2022 for other events) is shown with a purple rectangle. The area covered by the magnetic connectivity estimate represents the spatial and temporal uncertainties. We also show the HCS (red line) and CHs to explain these results better. The red and dark blue patches indicate respectively the positive and negative polarity regions of open magnetic field lines in the COCONUT simulation, while the gray areas indicate the CHs extracted from the SDO Carrington EUV maps using the EZSEG algorithm for events 1–3 (Caplan et al. 2016).

To this end, we combined the COCONUT coronal model with the EUHFORIA heliospheric model to compute the magnetic field lines from the Earth to the Sun. We then developed a way to quantify both the spatial and temporal uncertainty associated with this

computation. To validate our method, we selected four cases already studied in the literature and associated with high-speed-stream events coming from unambiguous coronal holes visible on the disk (Fig.17).

We always find a partial overlap with the assumed CH of origin. The extent of this overlap is 19% for event 1, 100% for event 2, 45% for event 3, and 100% for event 4. We looked at the polarity at Earth over the full Carrington rotation to better understand these results. We find that, on average, MHD simulations provide a very good polarity estimation, showing 69% agreement with real data for event 1, 36% for event 2, 68% for event 3, and 69% for event 4. For events 1 and 3, we can then explain the mixed results by the spatial and temporal uncertainty. An interesting result is that, for MHD models, minimum-activity cases appear to be more challenging because of the multiple recurrent crossings of the HCS, while maximum-activity cases appear easier because of the latitudinal extent of the HCS. A similar result was also found with Parker Solar Probe data in another study. In this work we have demonstrated that it is possible to use MHD models to compute magnetic connectivity and that this approach provides results of equal quality to those from the two-step ballistic method, with additional possibilities for improvements as the models integrate more critical physics.

4.5 Development aimed towards faster space weather models – Icarus

In this section we present the Icarus model and its connection with the COCONAT model.

4.5.1 The effect of adaptive mesh refinement and grid stretching on the magnetized coronal mass ejection model in Icarus, comparison with EUHFORIA

This work was presented in the publication: Baratashvili, T., Poedts, S., 2024, *Astronomy & Astrophysics*.

The impact of a CME at Earth is greatly affected by its internal magnetic field structure. The aim of this work is to enable the modeling of the evolution of the magnetic field configuration of the CME throughout its propagation in Icarus. Thus, we used Icarus to implement a magnetized CME model that is more realistic than the already available simple hydrodynamics cone CME model, allowing us to study the evolution of the magnetized CME during its interactions with the solar wind. The focus of the study is on the global magnetic structure of the CME and its evolution and interaction with the solar wind.

We analyzed the results from the performed simulations. The co-latitudinal magnetic field component is plotted at 1 AU for both Icarus and EUHFORIA simulations. The time series at Earth (L1) of the radial velocity, density, and different magnetic field components are plotted and compared (Fig. 18). The arrival time is better approximated by the EUHFORIA simulation, with the CME shock arriving 1.6 and 1.09 h later than in the AMR level 4 and 5 simulations, respectively. The profile features and variable strengths are best modeled by Icarus simulations with AMR level 4 and 5. The uniform, medium-resolution simulation with Icarus took 6.5 h wall-clock time, whereas with EUHFORIA, the most similar setup takes 18.5 h, when performed on 1 node with 2 Xeon Gold 6240 CPUs at 2.6 GHz (Cascadelake), 18 cores each, on the Genius cluster at KU Leuven. The Icarus simulation with AMR level 4 took only 2.5 h on the same computer infrastructure, while showing better resolved shocks and magnetic field features, when compared to the observational data and the reference uniform simulation results.

Our study shows that the arrival time is closer to the observed time in the EUHFORIA simulation, but the profiles of the different variables show more features and details in the

Icarus simulations. The simulations with AMR levels 4 and 5 offered the most detailed results. Considering the small difference in the modeled results and the large difference in terms of computational resources, the AMR level 4 simulation is considered to have displayed the most optimal performance. The gradients in the AMR level 4 results are sharper than those in the uniform simulations with both EUHFORIA and Icarus, while the AMR level 4 effective resolution is the most comparable to the standard resolution runs. The AMR level 3 simulation is 15 and 41 times faster than the Icarus and EUHFORIA uniform simulations, respectively; while the AMR level 4 simulation is about three and seven times faster than the uniform simulations, respectively.

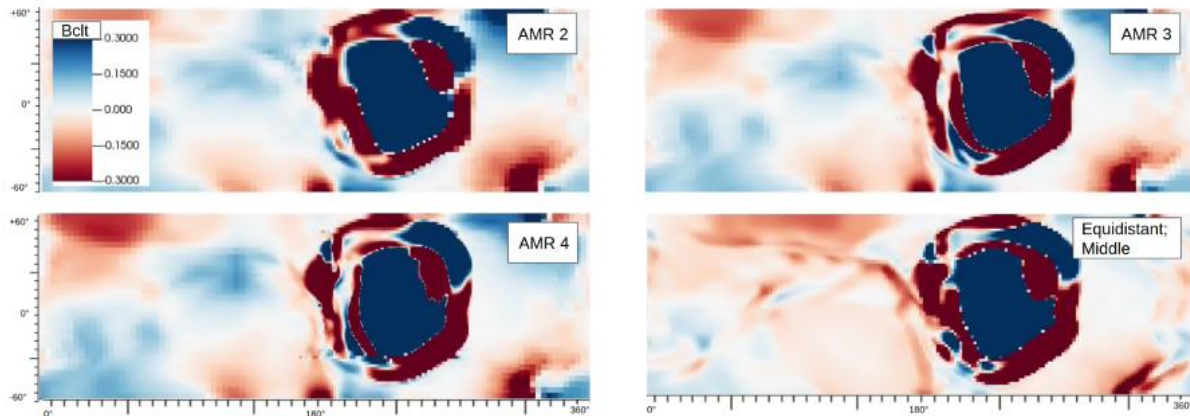


Figure 18. Figures given at the 1 au slice. The B_{cit} component of the magnetic field is plotted with the same scaling for all the figures for comparison purposes. AMR levels 2, 3, and 4 are used in the first three figures (two top panels and bottom left panel). The last figure shows results for the uniform medium-resolution grid simulation (bottom right panel).

4.5.2 The operationally ready full 3D magnetohydrodynamic model from the Sun to Earth: COCONUT+Icarus

This work was presented in the publication: Baratashvili, T., Brchnelova, M., Linan, L. et al., 2024, *Astronomy & Astrophysics*.

This study is focused on the novel full MHD chain from the Sun to Earth. Its goal is to demonstrate the capabilities of the full MHD modelling chain from the Sun to Earth by finalising the implementation of the full MHD coronal model into the COCONUT model and coupling it to the MHD heliospheric model Icarus. The resulting coronal model has significant advantages compared to the pre-existing polytropic alternative, as it includes more physics and allows for a more realistic modelling of bi-modal wind, which is crucial for heliospheric studies. In particular, we examine different empirical formulations for the heating terms in the MHD equations to determine an optimal one that would be able to mimic a realistic solar wind configuration most accurately. New heating source terms were implemented into the MHD equations of the pre-existing polytropic COCONUT model. A realistic specific heat ratio was applied. In this study, only thermal conduction, radiative losses, and approximated coronal heating function were considered in the energy equation. Multiple approximated heating profiles were examined to see the effect on the solar wind. The output of the coronal model was used to onset the 3D MHD heliospheric model Icarus. A minimum solar activity case was chosen as the first test case for the full MHD model. The numerically simulated data in the corona and the heliosphere were compared to observational products. First, we compared the density data to the available tomography data near the Sun and then the modelled solar wind

time series in Icarus was compared to OMNI 1-min data at 1 AU. Results. A range of approximated heating profiles were used in the full MHD coronal model to obtain a realistic solar wind configuration. The bi-modal solar wind was obtained for the corona when introducing heating that is dependent upon the magnetic field. The modelled density profiles are in agreement with the tomography data. The modelled wind in the heliosphere is in reasonable agreement with observations. Overall, the density is overestimated, whereas the speed at 1 AU is more similar to OMNI 1-min data. The general profile of the magnetic field components is modelled well (Fig.19), but its magnitude is underestimated.

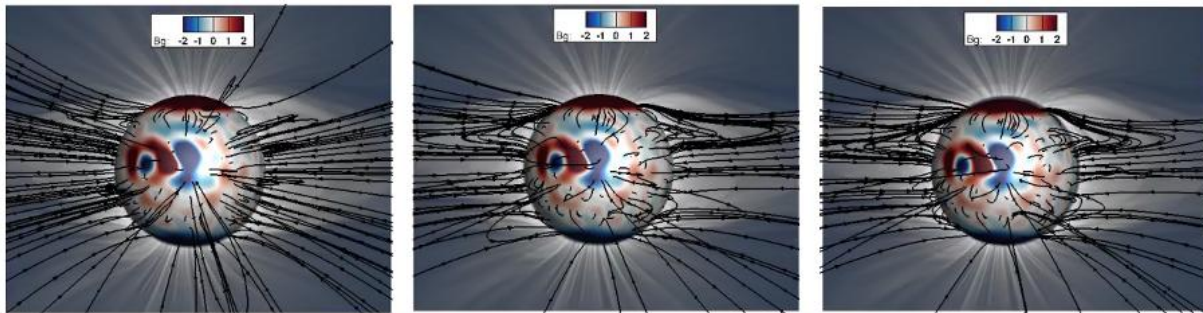


Figure 19. Full MHD COCONUT solutions with the indicated different heating profiles. The eclipse image is overlaid with the magnetic stream-lines from the COCONUT solution. The radial magnetic field is plotted on the solar surface.

4.6 Validation of EUHFORIA using of the radio density profiles and PSP observations

The extensive study was performed by K. Deshpande, one of the PhD students of the SWiM PI J. Magdalenic, and the manuscript in the submission process for Astronomy and Astrophysics: Deshpande, K., Magdalenic, J., Jebaraj, I., Senthamizh, P. V., Niemela, A., Krupar, V.

Knowledge on the characteristics of coronal electron density, at different distances from the Sun, is a very important topic in solar physics because it strongly influences the physical processes in the solar corona. Accurate mapping of coronal electron density is therefore of a crucial importance for understanding dynamics of solar corona. Majority of the methods used for estimation of coronal electron density have not been validated due to the absence of the close-to-the-Sun distances in situ observations closer to the Sun. Consequently, space weather forecasting models, which need the coronal density as an input, have also lacked proper validation. Newly available PSP in situ observations at distances close to the Sun, provide an opportunity to study the properties of plasma near the Sun and to validate both observational and modelling results.

The focus of this work is to evaluate the accuracy of estimation of the radio source positions in the 3D space using radio triangulation, and to validate the density estimated with radio observations and modelling with EUHFORIA with the PSP in-situ observations. In the study of type III radio bursts observed during the second PSP perihelion we employ the radio triangulation method and modelling. We use the method of radio triangulation to obtain the radio source positions in 3D. The state-of-the-art model EUHFORIA is used to estimate the electron densities at different positions. The density estimated with radio observations and with modelling with EUHFORIA is validated with the PSP in-situ observations.

The method of radio triangulation was found to be unable to find the accurate radio source positions in the case of the complex radio signal. The distance between the wave vectors was observed to be increasing with the decrease in the frequency for all studied type III radio bursts. This confirms the beam broadening observed in the case of type III bursts. The estimated radio densities were observed to be higher in comparison to the PSP in situ densities (Fig.20).

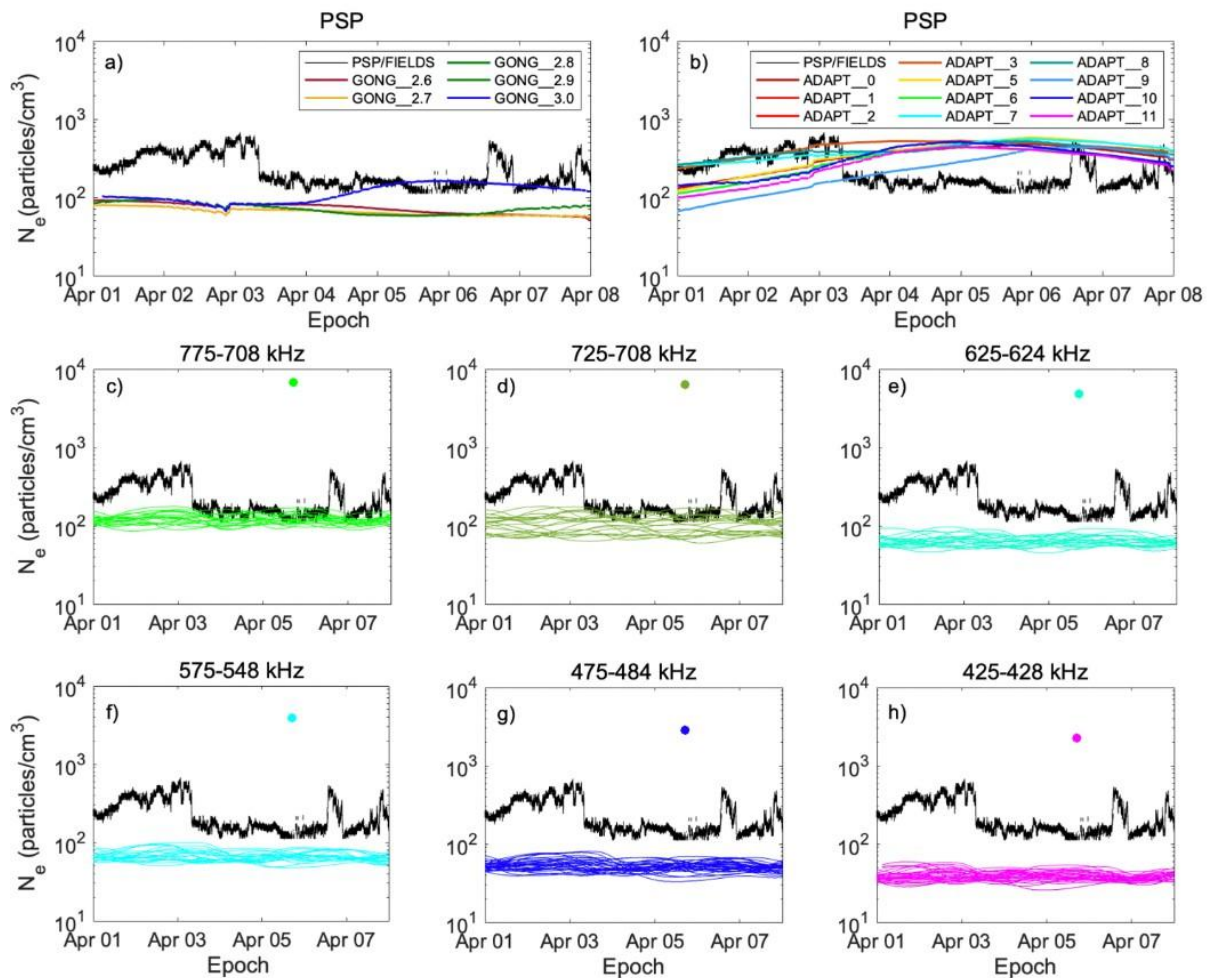


Figure 19. The comparison of the PSP/FIELDS electron density (black line) with EUHFORIA simulation results at various positions in the heliosphere. Panel (a) displays simulations at the PSP position using GONG magnetograms, with different coloured lines representing simulations performed with varying SSRs. The simulation using SSR = 3 Ro shows the best agreement with the in-situ data. Panel (b) shows simulations at the PSP position using all realizations of GONG ADAPT magnetic maps, which provide a better match than those using GONG magnetograms. Panels (c) to (h) present EUHFORIA results at radio source positions for different triangulation frequency pairs, with coloured points indicating the electron density at the respective radio frequencies (radio density). Radio densities are notably higher than the in-situ density, while the EUHFORIA results obtained at the radio source positions are underestimated

5. DISSEMINATION AND VALORISATION

The dissemination and valorisation of the project results was focused to presenting the project products such as lists of events studied and modelled in the SWiM project, new coronal models and also science to external scientists and the users (e.g. space weather forecasting centres, satellite operators, etc.).

Within the project dissemination we have:

- Contributed to the STCE (Solar Terrestrial Centre of Excellence) Newsletter when the milestones or some other exciting result was obtained.
- Provided the support to the new EUHFORIA users and collaborators.
- Introduced new models to the scientific public.
- Presented EUHFORIA, COCONUT and Icarus at different general public presentation.

In the framework of the SWiM project a large number of invited talks, presentations and posters was presented at different international conferences. The studies that were conducted in the framework of the SWiM project were presented at international and national conferences, by project members and a large number of the involved students whose PhD projects had an overlap with the SWiM topics,

We list here some of the largest conferences at which the SWiM project work was presented:

- EGU General Assembly: EGU 2019, 2020, 2021, 2022, 2023
- European Space Weather Week: ESWW17 in 2020, ESWW18 in 2021, ESWW19 in 2022, ESWW20 in 2023, ESWW21 in 2024
- European Solar Physics Meeting: ESPM 2024
- CESRA Workshop 2023
- AGU annual meetings: AGU 2020, 2021, 2022, 2023, 2024

Together with the regular teleconferences monthly in person meetings were organized alternatively at ROB or KU Leuven. The follow-up committee members occasionally participated in the regular teleconferences.

6. PUBLICATIONS

Direct output of the project were also more than 40 scientific publications in the refereed journals.

List of publications of the SWiM project:

1. Annie John, L., Nyberg, S., Vuorinen, L. et al., 2024, Journal of Space Weather & Space Climate, Vol. 14, id.15, 9 pp.
2. Arshad, K., Poedts, S., Dahshan, A., 2022, AIP Advances, Vol. 12, Issue 10, 8 pp.
3. Baratashvili, T., Brchnelova, M., Linan, L. et al., 2024, A & A, Vol. 690, id.A184, 12 pp.
4. Baratashvili, T., Grison, B., Schmieder, B. et al., 2024, A & A, Vol. 689, id.A98, 16 pp.
5. Baratashvili, T., Poedts, S., 2024, A & A, Vol. 683, id.A81, 11 pp.
6. Baratashvili, T., Verbeke, C., Keppens, R. et al., 2023, Sun & Geosphere, 15/2, 49-54.
7. Baratashvili, T., Verbeke, C., Wijsen, N. et al., 2022, A & A, Vol. 667, id.A133, 12 pp.
8. Brchnelova, M., Gudiksen, B., Carlsson, M. et al., 2025, A & A, Vol. 693, id.A74, 6 pp.
9. Brchnelova, M., Kuźma, B., Perri, B. et al., 2022, APJ Supplement Series, Vol. 263, Issue 1, id.18, 23 pp.
10. Brchnelova, M., Kuźma, B., Zhang, F. et al., 2023, Sun & Geosphere, 15/2, 59-63.
11. Brchnelova, M., Kuźma, B., Zhang, F. et al., 2023, A & A, Vol. 676, id.A83, 13 pp.
12. Brchnelova, M., Kuźma, B., Zhang, F. et al., 2023, A & A, Vol. 678, id.A117, 15 pp.
13. Brchnelova, M., Pueschel, M. J., Poedts, S., 2024, Physics of Plasmas, Vol. 31, 10 pp.
14. Brchnelova, M., Zhang, F., Leitner, P., et al., 2022, Journal of Plasma Physics, Vol. 88
15. Chen, W., Yuan, D., Feng, X. et al., 2025, Advances in Space Research, Vol. 75, pp. 2449-2460.
16. Deshpande, K., Magdalenic, J., Jebaraj, I., Senthamizh, P. V., Niemela, A., Krupar, V., in a process of submission to A & A
17. Dhib, R., Sharma, V., Lani, A. et al., 2024, SoftwareX, Volume 28, id.101943.
18. Ding, Z., Li, G., Mason, G. et al., 2024, A & A, Vol. 681, id.A92, 15 pp.
19. Ding, Z., Li, G., Santa Fe Dueñas, A. et al., 2023, Journal of Geophysical
20. Ding, Z., Li, G., Wijsen, N. et al., 2024, APJ Letters, Vol. 964, Issue 1, id.L8, 7 pp.
21. Ding, Z., Wijsen, N., Li, G. et al., 2022, A & A, Vol. 668, id.A71, 13 pp.
22. Dumbadze, G., Shergelashvili, B. M., Khodachenko, M. L. et al., 2024, A & A, Vol. 683, 15 pp.
23. Echeverría-Veas, S., Moya, P. S., Lazar, M. et al., 2024, APJ, Vol. 975, 12 pp.
24. Gerekos, C., Steinbrügge, G., Jebaraj, I. C. et al., 2024, A & A, Vol. 683, id.A56, 14 pp.
25. Goedbloed, H., Poedts, S., 2024, Research Notes of the AAS, Vol. 8, Issue 3, id.60
26. Guo, J. H., Linan, L., Poedts, S. et al., 2024, A & A, Vol. 683, id.A54, 14 pp.
27. Guo, J. H., Linan, L., Poedts, S. et al., 2024, A & A, Vol. 690, id.A189, 10 pp.
28. Guo, J. H., Ni, Y. W., Guo, Y. et al., 2024, APJ, Vol. 961, Issue 1, id.140, 17 pp.
29. Guo, J. H., Ni, Y. W., Zhong, Z. et al., 2023, APJ Supplement Series, Vol. 266, 20 pp.
30. Guo, J. H., Qiu, Y., Ni, Y. W. et al., 2023, APJ, Vol. 956, Issue 2, id.119, 16 pp.
31. Hofmeister, S. J., Asvestari, E., Guo, J. et al., 2022, A & A, Vol. 659, id.A190, 18 pp.
32. Hosteaux, S., Chané, E., Poedts, S., 2021, Geosciences, Vol. 11, Issue 8, id.314
33. Hosteaux, S., Rodriguez, L., Poedts, S., 2022, Advances in Space Research, Vol. 70, p. 1684-1719.
34. Husidic, E., Lazar, M., Fichtner, H. et al., 2021, A & A, Vol. 654, id.A99, 10 pp.
35. Husidic, E., Scherer, K., Lazar, M. et al., 2022, APJ, Vol. 927, Issue 2, id.159, 10 pp.
36. Husidic, E., Wijsen, N., Baratashvili, T. et al., 2024, Journal of Space Weather and Space Climate, Vol. 14, 12 pp.
37. Husidic, E., Wijsen, N., Linan, L. et al., 2024, APJ Letters, Vol. 976, Issue 2, 12 pp.
38. Javed, S., Rubab, N., Zaheer, S. et al., 2023, Space Weather, Vol. 21, Issue 10

39. Jebaraj, I. C., Kouloumvakos, A., Dresing, N. et al., 2023, A & A, Vol. 675, 21 pp.
40. Jebaraj, I. C., Kouloumvakos, A., Magdalenic, J. et al., 2021, A & A, Vol. 654, 15 pp.
41. Jebaraj, I. C., Krasnoselskikh, V., Pulupa, M. et al., 2023, APJ Letters, Vol. 955, 11 pp.
42. Jebaraj, I. C., Magdalenic, J., Krasnoselskikh, V. et al., 2023, A & A, Vol. 670, 16 pp.
43. Jebaraj, I. C., Magdalenic, J., Podladchikova, T. et al., 2021, A & A, Vol. 639, 16 pp.
44. Kennis, S., Perri, B., Poedts, S., 2024, A & A, Vol. 691, id.A257, 11 pp.
45. Koehn, G. J., Desai, R. T., Davies, E. E. et al., 2022, APJ, Vol. 941, Issue 2, 13 pp.
46. Kouloumvakos, A., Rouillard, A., Warmuth, A. et al., 2021, APJ, Vol. 913, 12 pp.
47. Kraskiewicz, J., Murawski, K., Zhang, F. et al., 2023, Solar Physics, Vol. 298, Issue 1
48. Kumar, M., Murawski, K., Kuźma, B. et al., 2024, APJ, Vol. 975, Issue 1, id.3, 10 pp.
49. Kuźma, B., Brchnelova, M., Perri, B. et al., 2022, Magnetohydrodynamics 58, No. 4, 509-514.
50. Kuźma, B., Brchnelova, M., Perri, B. et al., 2022, AMOS 2022 conference proceedings, Vol. 2022, pp. 1622 - 1628.
51. Kuźma, B., Brchnelova, M., Perri, B. et al., 2023, APJ, Vol. 942, Issue 1, id.31, 14 pp.
52. Lario, D., Wijzen, N., Kwon, R. Y. et al., 2022, APJ, Vol. 934, Issue 1, id.55, 27 pp.
53. Lazar, M., López, R. A., Moya, P. S. et al., 2023, A & A, Vol. 670, id.A85, 13 pp.
54. Lazar, M., López, R. A., Poedts, S. et al., 2023, Solar Physics, Vol. 298, Issue 5
55. Lazar, M., López, R. A., Poedts, S. et al., 2023, Physics of Plasmas, Vol. 30, 14 pp.
56. Lazar, M., López, R. A., Shaaban, S. M. et al., 2022, Frontiers in Astronomy & Space Sciences, Vol. 8, id.249
57. Lazar, M., Shaaban, S. M., López, R. A. et al., 2022, Astrophysics & Space Science, Volume 367, Issue 10, article id.104
58. Li, X., Senthamizh Pavai, V., Shukhobodskaia, D. et al., 2024, Space Weather, Vol. 22, Issue 1, article id. e2023SW003499
59. Linan, L., Baratashvili, T., Lani, A. et al., 2025, A & A, Vol. 693, id.A229, 19 pp.
60. Linan, L., Maharana, A., Poedts, S. et al., 2024, A & A, Vol. 681, id.A103, 20 pp.
61. Linan, L., Regnault, F., Perri, B. et al., 2023, A & A, Vol. 675, id.A101, 20 pp.
62. López, R. A., Micera, A., Lazar, M. et al., 2022, APJ, Vol. 930, Issue 2, id.158, 8 pp.
63. Maharana, A., Cramer, W. D., Samara, E. et al., 2024, Space Weather, Vol. 22, Issue 5, article id. e2023SW003715.
64. Maharana, A., Isavnin, A., Scolini, C. et al., 2022, Advances in Space Research, Vol. 70, Issue 6, p. 1641-1662.
65. Maharana, A., Linan, L., Poedts, S. et al., 2024, A & A, Vol. 691, id.A146, 27 pp.
66. Maharana, A., Scolini, C., Schmieder, B. et al., 2023, A & A, Vol. 675, id.A136, 19 pp.
67. Masson, A., Fung, S. F., Camporeale, E. et al., 2024, Advances in Space Research
68. Mierla, M., Zhukov, A. N., Berghmans, D. et al., 2022, A & A, Vol. 662, id.L5, 11 pp.
69. Moya, P. S., López, R. A., Lazar, M. et al., 2022, APJ, Vol. 937, Issue 2, id.49, 9 pp.
70. Murawski, K., Musielak, Z. E., Poedts, S. et al., 2022, Astrophysics and Space Science, Vol. 367, Issue 11, article id.111.
71. Niedziela, R., Murawski, K., Kadowaki, L. et al., 2022, A & A, Vol. 668, id.A32, 11 pp.
72. Niedziela, R., Murawski, K., Poedts, S. et al., 2021, A & A, Vol. 652, id.A124, 10 pp.
73. Niedziela, R., Murawski, K., Poedts, S. et al., 2024, A & A, Vol. 691, id.A254, 7 pp.
74. Niemela, A., Wijzen, N., Aran, A. et al., 2023, A & A, Vol. 679, id.A93, 21 pp.
75. Niemela, A., Wijzen, N., Aran, A. et al., 2024, APJ Letters, Vol. 967, Issue 2, 10 pp.
76. Nourina, N., Rozina, Ch., Iqbal, Z. et al., 2025, Physica Scripta, Vol. 100, Issue 1, id.015615, 14 pp.
77. Pelekhata, M., Murawski, K., Poedts, S. et al., 2021, A & A, Vol. 652, id.A114, 8 pp.
78. Pelekhata, M., Murawski, K., Poedts, S., 2023, A & A, Vol. 669, id.A47, 13 pp.
79. Pelekhata, M., Murawski, K.; Poedts, S., 2024, A & A, Vol. 689, id.A155, 6 pp.

80. Perri, B., Kuźma, B., Brchnelova, M. et al., 2023, APJ, Vol. 943, Issue 2, id.124, 21 pp.
81. Perri, B., Leitner, P., Brchnelova, M. et al., 2022, APJ, Vol. 936, Issue 1, id.19, 23 pp.
82. Perri, B., Schmieder, B., Démoulin, P. et al., 2023, APJ, Vol. 955, Issue 1, id.50, 23 pp.
83. Prete, G., Niemela, A., Schmieder, B. et al., 2024, A & A, Vol. 683, id.A28, 12 pp.
84. Rodriguez, L., Barnes, D., Hosteaux, S. et al., 2022, Solar Physics, Vol. 297, Issue 2
85. Rodriguez, L., Shukhobodskaya, D., Niemela, A. et al., 2024, A & A, Vol. 689, 16 pp.
86. Rodriguez, L., Warmuth, A., Andretta, V. et al., 2023, Solar Physics, Vol. 298, Issue 1
87. Sabri, S., Poedts, S., 2024, Frontiers in Astronomy and Space Sciences, Vol.11, 14pp.
88. Sabri, S., Poedts, S., 2024, Scientific Reports, Vol. 14, Issue 1, 30723.
89. Sabri, S., Poedts, S., Ebadi, H., 2023, APJ, Vol. 944, Issue 1, id.72, 12 pp.
90. Samara, E., Laperre, B., Kieokaew, R. et al., 2022, APJ, Vol. 927, Issue 2, 19 pp.
91. Samara, E., Arge, C. N., Pinto, R. F. et al., 2024, APJ, Vol. 971, Issue 1, id.83, 17 pp.
92. Samara, E., Magdalenic, J., Rodriguez, L. et al., 2022, A & A, Vol. 662, id.A68, 19 pp.
93. Samara, E., Pinto, R. F., Magdalenic, J. et al., 2021, A & A, Vol. 648, id.A35, 15 pp.
94. Sarkar, R., Pomoell, J., Kilpua, E. et al., 2024, APJ Supplement Series, Vol. 270, 16 pp.
95. Senthamizh, P. V., J. Magdalenic, J., Rodriguez, L., Poedts, S., and Samara, E., in a process of submission to A & A
96. Schmieder, B., Guo, J., Poedts, S., 2024, Reviews of Modern Plasma Physics, Vol. 8, Issue 1, article id.27.
97. Scolini, C., Dasso, S., Rodriguez, L. et al., 2021, A & A, Vol. 649, id.A69, 20 pp.
98. Scolini, C., Winslow, R. M., Lugaz, N. et al., 2021, APJ Letters, Vol. 916, 14 pp.
99. Scolini, C., Winslow, R. M., Lugaz, N. et al., 2023, APJ, Vol. 944, Issue 1, id.46, 17 pp.
100. Seba, E. B., Poedts, S., 2025, Advances in Space Research, Vol. 75, Issue 1, pp. 918-935.
101. Shaaban, S. M., Lazar, M., López, R. A. et al., 2024, A & A, Vol. 692, id.L6, 6 pp.
102. Shaaban, S. M., López, R. A., Lazar, M. et al., 2024, A & A, Vol. 691, id.A86, 11 pp.
103. Shaifullah, G. M., Magdalenic, J., Tiburzi, C. et al., 2023, Advances in Space Research, Vol. 72, Issue 12, p. 5298-5310.
104. Shergelashvili, B. M., Philishvili, E., Buitendag, S. et al., 2022, A & A, Vol. 662, 10 pp.
105. Soni, S. L., Maharana, A., Guerrero, A. et al., 2024, A & A, Vol. 686, id.A23, 13 pp.
106. Sorokina, D., Van Doorselaere, T., Talpeanu, D. -C. et al., 2024, A & A, Vol. 682, 8 pp.
107. Talpeanu, D. C., Poedts, S., D'Huys, E. et al., 2022, A & A, Vol. 658, id.A56, 14 pp.
108. Talpeanu, D. C., Poedts, S., D'Huys, E. et al., 2022, A & A, Vol. 663, id.A32, 13 pp.
109. Valentino, A., Magdalenic, J., 2024, A & A, Vol. 690, id.A137, 21 pp.
110. Valentino, A., Magdalenic, J., A & A, 2025, to be submitted
111. Verbeke, C., Baratashvili, T., Poedts, S., 2022, A & A, Vol. 662, id.A50, 11 pp.
112. Wagner, A., Bourgeois, S., Kilpua, E. K. J. et al., 2024, A & A, Vol. 683, id.A39, 11 pp.
113. Wagner, A., Kilpua, E. K. J., Sarkar, R. et al., 2023, A & A, Vol. 677, id.A81, 12 pp.
114. Wagner, A., Price, D. J., Bourgeois, S. et al., 2024, Frontiers in Astronomy and Space Sciences, Vol. 11, id. 1383072.
115. Wagner, A., Price, D. J., Bourgeois, S. et al., 2024, A & A, Vol. 692, id.A74, 11 pp.
116. Wang, H. P., Guo, J. H., Yang, L. P. et al., 2025, A & A, Vol. 693, id.A257, 17 pp.
117. Whitman, K., Egeland, R., Richardson, I. G. et al., 2023, Advances in Space Research, Vol. 72, Issue 12, p. 5161-5242.
118. Wijzen, N., Lario, D., Sánchez-Cano, B. et al., 2023, APJ, Vol. 950, Issue 2, 10 pp.
119. Wijzen, N., Li, G., Ding, Z. et al., 2023, Journal of Geophysical Research: Space Physics, Vol. 128, Issue 3, article id. e2022JA031203.
120. Winslow, R. M., Scolini, C., Jian, L. K. et al., 2022, Frontiers in Astronomy and Space Sciences, Vol. 9, id.422.
121. Zenteno-Quinteros, B., Moya, P. S., Lazar, M. et al., 2023, APJ, Vol. 954, 14 pp.

122. Zimbardo, G., Ying, B., Nisticò, G. et al., 2023, A & A, Vol. 676, id.A48, 11 pp.
123. Zhao, J., Malaspina, D. M., Dudok de Wit, T. et al., 2022, APJ Letters, Vol. 938, 9 pp.